Check for updates

Energy &
Environmental
Science

rsc.li/ees

Volume 11
Number 4
April 2018
Pages 719-1000

ISSN 1754-5706

ROYAL SOCIETY
OF CHEMISTRY

REVIEW ARTICLE
Yuekun Lai, Zhiqun Lin et al.
Graphene aerogels for efficient energy storage and conversion

ROYAL SOCIETY
OF CHEMISTRY

rsc.li/ees

Palladium alloys used as electrocatalysts for the oxygen reduction reaction

Tianlei Wang[a], Arunabhiram Chutia[c], Dan J.L. Brett[d], Paul R. Shearing[d], Guanjie He[a,c,d]*, Guoliang Chai[b]* and Ivan P. Parkin[a]*

a. Christopher Ingold Laboratory, Department of Chemistry, University College London, 20 Gordon Street, London WC1H 0AJ, U.K. Email: g.he@ucl.ac.uk ; i.p.parkin@ucl.ac.uk

b. State Key Laboratory of Structural Chemistry, Fujian Institute of Research on the Structure of Matter, Chinese Academy of Sciences (CAS), Fuzhou, 350002 Fujian, P.R. China. Email: g.chai@fjirsm.ac.cn

c. School of Chemistry, University of Lincoln, Brayford Pool, Lincoln, LN6 7TS, UK

d. Electrochemical Innovation Lab (EIL), Department of Chemical Engineering, University College London (UCL), London WC1E 7JE, UK.

Abstract

Palladium-based alloy materials as cathodes for the reduction of oxygen are regarded as potential substitutes for platinum-based catalysts in fuel cells. In this work, we present the scientometric analysis and critically review the use of Pd alloys for the oxygen reduction reaction (ORR). Through scientometric analysis, publication information, research fronts and hotspots are identified. For the critical review, reaction mechanisms in different media are discussed, with the aid of volcano plots to show the general principles for catalyst modifications to maximise the ORR. Influencing factors, including alloying, structure, strain and ligand, particle size, crystal facet and dealloying are considered with a view to informing the theoretical feasibility to enhance ORR activity. In addition, Pd-based alloys synthesized by different methods are presented and compared in terms of ORR activities. Future research directions are discussed and possible approaches to the mass production for industrialization are also proposed.

Broader context

With the rising global population and increasing energy demands, fuel cells are attracting considerable interests as alternative energy conversion devices for highly efficient direct chemical-to-electrical energy conversion. The oxygen reduction reaction (ORR) at the cathode is a multi-electron, multi-step reaction with sluggish kinetics. Platinum represents the most widely explored ORR electrocatalysts for its excellent catalytic performance. Compared to Pt, the research on Pd as the ORR catalysts is relatively limited. However, with the advantages of lower cost, more abundance and better methanol tolerance, Pd-based materials have promising prospects to replace Pt-based ones. Herein, we combine the scientometric analysis and critical review method to present a deep and broad overview of Pd alloys for ORR. Through scientometric analysis, the developments, fronts and hotspots in this field are identified. For the critical review, the mechanisms in different solutions, volcano plots of the ORR catalysts and the crucial elements to enhance the electrocatalytic performance are summarized. Additionally, various synthesis methods of Pd-metal alloy materials are concluded and compared. Finally, we propose perspectives and suggestions for the further development of Pd alloys used as the ORR electrocatalysts. This work aims to provide a comprehensive and critical insight and indicate a clear direction for future research.

1. Introduction

The oxygen reduction reaction (ORR), one of the key chemical reactions in fuel cells and metal-air batteries, has been intensively investigated over the last several decades[1-3]. The research of ORR catalysts can be traced back to the 1970s, where most attention was focused on the platinum (Pt) based catalysts[4-6]. The Pt-based catalysts set the benchmarks due to their excellent ORR performance and stability, and are widely used as cathode electrocatalysts in practical fuel cells.[7] However, there are several obstacles for commercialization: (1) the high price and the scarcity of Pt materials; (2) the methanol crossover effect and poor methanol tolerance, which leads to low cell performance and efficiency when using Pt-based catalysts in direct methanol fuel cells (DMFCs)[8], and (3) easy poisoning by impurities, such as CO and chloride ions in electrolytes. In recent years there have been attempted to reduce the amount of Pt catalysts but it has been found that under cathodic conditions Pt can easily migrate and aggregate on the carbon support. Additionally, if the particles are smaller in size then they can dissolve to form Pt cations, which then can deposit on other Pt particles causing them to grow and deactivate, leading to the use of a large amount of Pt metals. Therefore, research effort has also been directed at the development of alternatives, such as other noble metals with relatively low-cost, non-noble metal materials and even metal-free catalysts. The emergence of these studies has greatly enriched the types of ORR electrocatalysts and paved several pathways for practical applications.

Amongst these, palladium (Pd) based materials have attracted extensive interests as alternative electrocatalysts because of their comparable properties and slightly lower cost compared to Pt. For instance, the average prices of Pd and Pt in the last ten years (from 1 August 2010 to 1 August 2020) are \$910.62 and \$1230.96 per troy oz, respectively (www.platinum.matthey.com/prices). Specifically, both Pd and Pt are platinum group metals, and they are adjacent in the periodic table, resulting in similar chemical properties. For example, both are inactive and stable in air and humid environment at room temperature and are easy to form alloys with other metals. Also, the physical properties (such as colour, appearance, melting point, hardness and ductility) are similar. And Pd has a very similar electronic property to Pt.[9] Catalysts based on Pd were claimed to have higher methanol tolerance than Pt-based catalysts[10], more stable than non-precious metal catalysts in acidic media and highly tolerant towards CO poisoning[11]. Unlike Pt/C, Pd-based electrocatalysts did not show any methanol

oxidation peak above 0.7 V.[12] The methanol oxidation on Pt/C caused the onset of net cathode current to shift negatively and resulted in a significant increase in overpotential.[13] Thus, Pd-based electrocatalysts tend to exhibit better ORR selectivity than Pt-based ones in the presence of methanol.

The study of Pd-based catalysts can be traced back to the first half of the last century. In the early studies, researchers mostly investigated the catalytic oxidation performance, such as methanol oxidation,[14] ethylene oxidation,[15] carbon monoxide oxidation,[16] formate oxidation,[17] as well as various physicochemical properties[18-21] and structural characteristics.[22, 23] For pure Pd catalyst due to its intrinsic properties, it is difficult to achieve the catalytic performance for ORR and stability close to that of Pt. For example, the binding ability of Pd to oxygen is too strong, which hinders the reduction of oxygen. The ORR activity of a poly-Pd is about five times lower than that of a poly-Pt in $HClO_4$ solutions.[24] In addition, by alloying with other elements (especially transition metals), the ORR activity of Pd based catalysts can be enhanced dramatically[25] and the production cost of electrocatalysts can be further reduced.

Overall, a large and growing number of studies have investigated the role of Pd alloys as ORR catalysts and strive to enhance the activity to match, or even exceed Pt-based catalysts. Herein scientometric analysis and traditional review methods are combined with an aim to provide a comprehensive and critical insight and indicate a clear direction for future research in this area. In terms of scientometric analysis, based on Bibliometrix/Biblioshiny R-package[26], Citespace[27, 28] and VOSviewer[29] software, annual production, the top 10 sources and countries by publications, co-citation and keywords analysis, and co-keywords networks are discussed. In terms of the conventional review, this work elucidates the development of ORR mechanisms in different media, volcano plots in previously reported ORR electrocatalysts, the theoretical possibility of an enhancement in ORR activity and the recent advances in Pd-based electrocatalysts.

2. Scientometric analysis on Pd alloys for ORR

Before 1970, although there have been several reports on the ORR of Pd alloys,[24, 30, 31] most of them were not exhaustive and systematic. Based on the database in the Web of Science from 1970 to 2020, a total of 400 articles were obtained on the Pd alloys for the ORR. As shown in

Figure 1, the first report appeared in 1997, and the studies in this field have grown significantly in the past decade. In this study, Pattabiraman *et al.* dispersed Pd catalysts on various carbon supports and reported their ORR activity in alkaline media for the first time.[25] Also, amorphous PdP alloy catalysts for ORR in alkaline media were reported by Podestá *et al.*[32] In 2004, Savadogo *et al.* proposed active Pd based alloy catalysts for ORR in acidic media for the first time and showed that the PdCo alloy (the atomic ratio of Pd to Co is 72:28) may exhibit better performance for ORR than Pt materials.[33] Since then, the relevant research in this area has gradually increased.[34-36] For example, Shao *et al.* synthesized PdFe nanoparticles for ORR and found that the surface-specific activity of the PdFe alloys is related to the Pd−Pd bond distance: the shorter the bond distance, the higher the activity.[36]
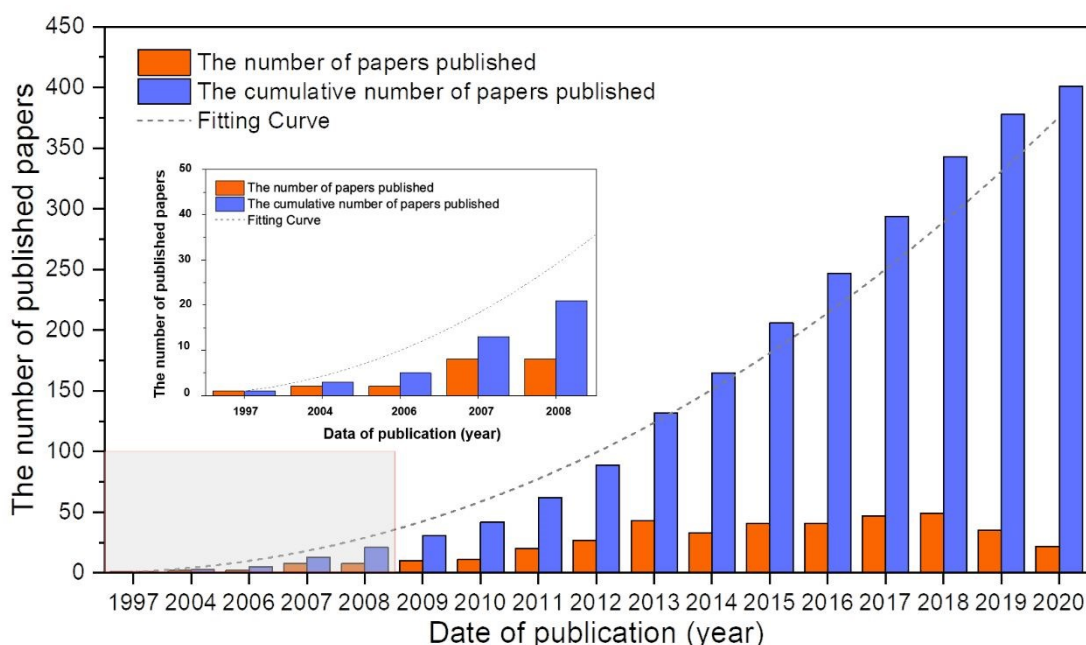
Figure 1. Number of Web of Science (WOS)-based research literature on Pd alloys for the ORR. Source: Literature statistics from the WOS Platform.
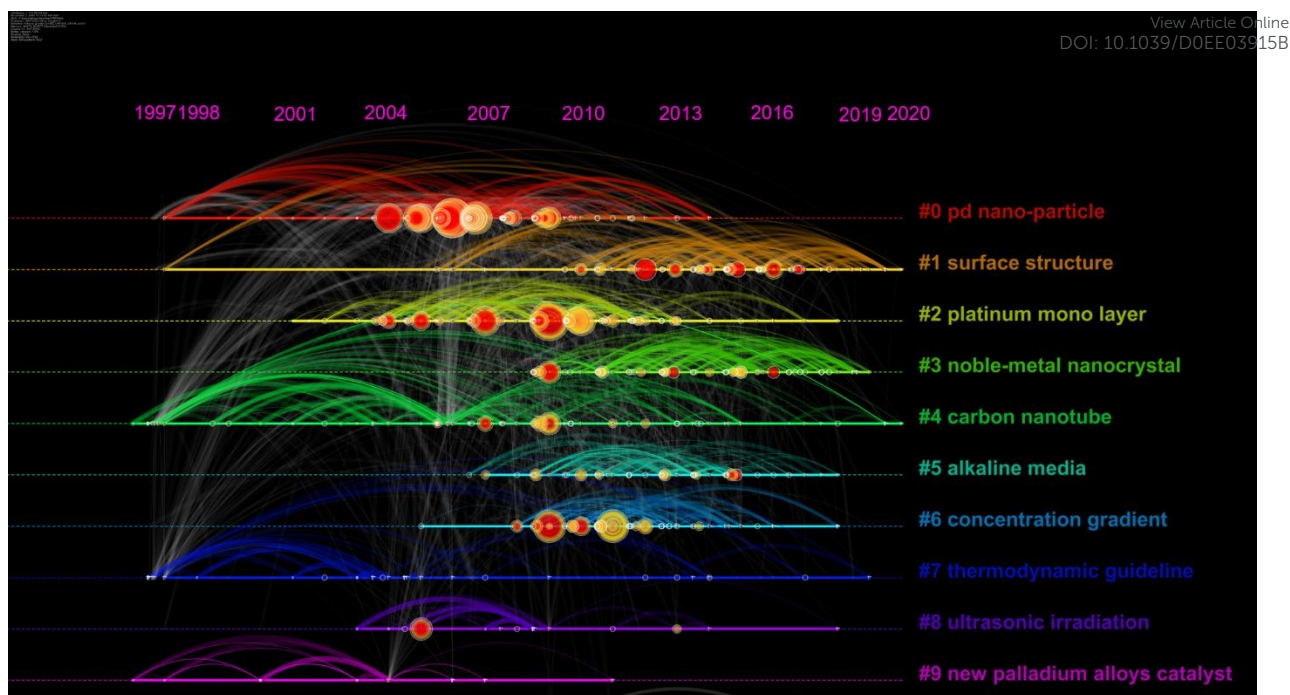
Figure 2. A timeline visualization for the network of co-citation and keywords co-occurrence of the literature about Pd alloys for the ORR between 1997 and 2020.

Table 1. The main information about the largest four clusters.

Cluster ID	Size	Silhouette	Mean cite year
#0 Pd nano-particle	103	0.621	2007
#1 surface structure	93	0.578	2014
#2 platinum mono layer	88	0.502	2009
#3 noble-metal nanocrystal	82	0.655	2014

Based on Citespace software, taking advantage of cluster analysis of title terms, emerging trends and new developments in this field can be easily identified, as shown in Figure 2. Clusters (groupings) could be found and numbered in the size descending order of the cluster size. For example, the size of cluster #0 (Pd nano-particle) is the largest. Each point in the graph represents a node, and the node means keywords or references. For 'tree ring' shaped nodes, the number of citations the article received in a particular year affects the thickness of nodes; a red ring presents a particular year denotes a citation burst (a surge of citation). The network indicates the co-citation and co-occurrence of keywords. The network

of different types of entities has different meanings. For instance, lines that connect nodes in a cited reference network are co-citation links. Table 1 presents the information about the largest four clusters by size. The silhouette value reflects the homogeneity and consistency of the cluster.

Pd nano-particle (cluster #0) is the focus of research in this field. The study of surface structure (cluster #1) exhibits a good trend for possible future development. Alloyed with platinum (cluster #2), carbon nanotube as the carrier (cluster #4), and applied in alkaline media (cluster #5) are also the hotspots.

Figure 3. Co-keyword network visualization on Pd alloys for ORR research. Note: (a) network visualization based on co-keyword; (b) density visualization map based on co-keywords.

The keywords summarize the main purpose of the literature to a certain extent, and they can comprehensively interpret its content. Based on the VOSviewer software, co-keyword network visualization maps are shown in Figure 3 to understand the hotspots and directions in this field. Although there is no specific quantitative data, the direct connection of keywords and the frequency and proportions of the research can be clearly identified from Figure 3(a) and 3(b), respectively. For the topic, "Palladium (Pd) alloy(s) for ORR", the keywords highlighted in the figure are: "nanoparticles", "electrocatalysts", "stability", "enhancement" and through the co-keyword network, the top research directions and underlying problems in this field are revealed, which are namely:

(1) Nanoparticles of palladium alloy(s) prepared by various methods are used for ORR catalysis. Catalysts with different morphologies such as nanowire, core-shell and monolayer are widely studied.

(2) The main metals alloyed with Pd are Pt, Co, Au, Fe, Ni and Cu.

(3) Stability and catalytic activity are still the focus in this field. Developing methods to realize comparable performance with Pt is one of the key difficulties in this research.

(4) The pursuit of simpler and more effective synthetic methods, such as facile synthesis and one-pot synthesis.

(5) The combination of carbon material supports, such as graphene, reduced graphene oxide, carbon nanotubes, *etc.*

(6) In addition to oxygen reduction, Pd alloy catalysts are widely used in formal acid oxidation, methanol oxidation, and ethanol oxidation. The preparation of dual-functional catalysts, which have both oxygen reduction activity and organic oxidation activity, is an interesting research topic.

(7) There is limited research on mechanism and kinetics, and more in-depth work is needed.

3. ORR mechanisms

The ORR mechanisms on noble metal surfaces, such as Pd and Pt, have not been completely understood despite the intensive studies over the past few decades.[37] In general, due to the similarities of Pd and Pt, the ORR processes on these two electrocatalysts are basically similar, that is, this reaction starts with the adsorption of molecular oxygen on the catalyst surface, and then two mechanisms have been generally accepted: one is a direct four-electron mechanism where the O_2 is reduced directly to water without the production of H_2O_2; the other is a series of four-electron mechanism where the O_2 is reduced to H_2O_2 and then further reduced to water. Depending on the pH value of the electrolyte, the electrochemical reduction of oxygen follows different pathways. Specifically, in the acidic solution, the reaction is:

$$O_2 + 4H^+ + 4e^- \rightarrow 2H_2O \tag{1}$$

While in the alkaline solution, the overall reaction is:

$$O_2 + 2H_2O + 4e^- \rightarrow 4OH^- \tag{2}$$
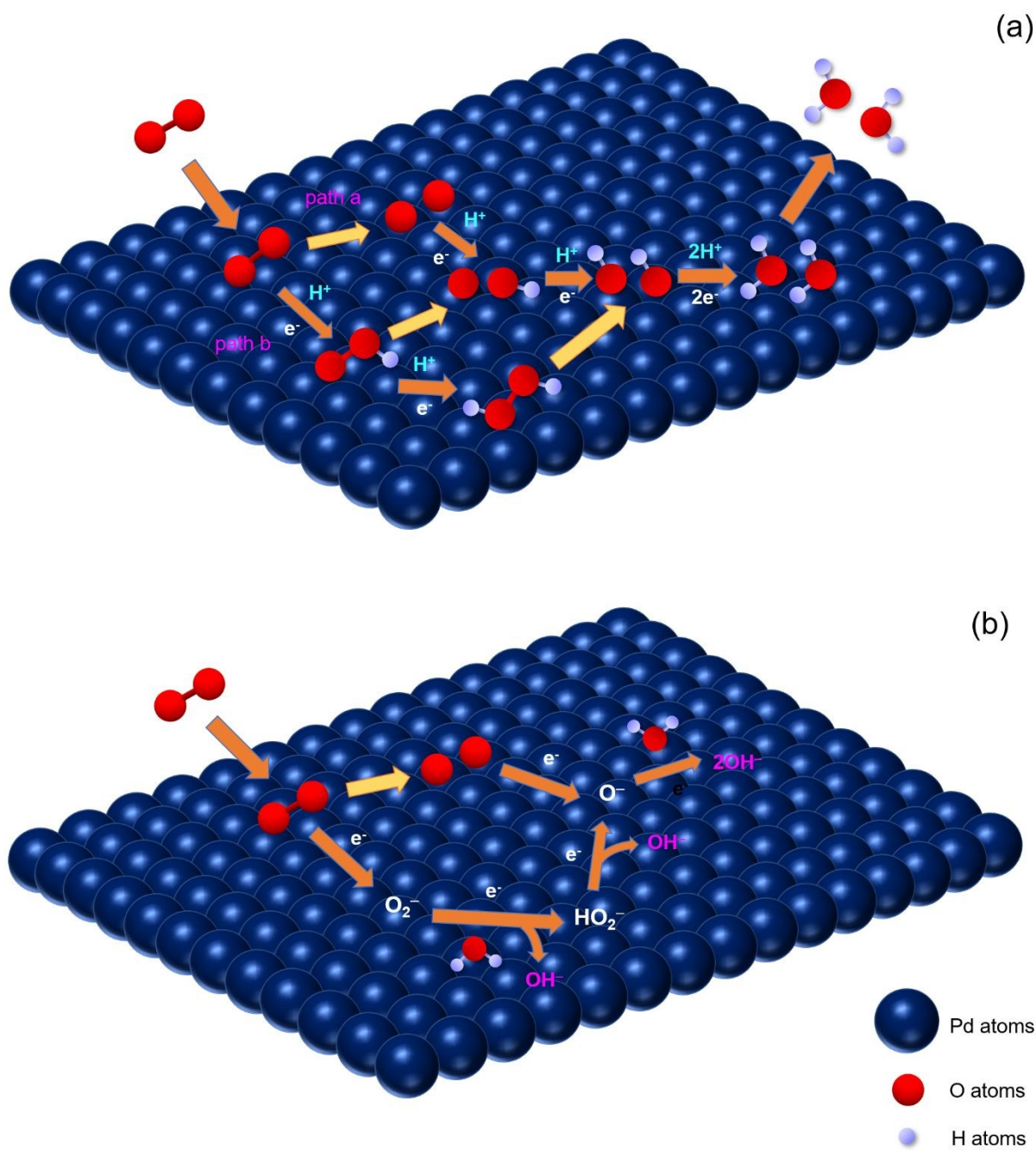
Figure 4. Schematic diagram of mechanisms for ORR on Pd in acidic (a) and alkaline (b) media, respectively.

In acidic media, the ORR process undergoes the following steps[38]:

$$O_{2(g)} \rightarrow O_{2(ads)} \tag{3}$$

Pathway a:

$$O_{2(ads)} \rightarrow 2O_{(ads)} \qquad (4)$$

$$O_{ads} + H^+ + e^- \rightarrow OH_{(ads)} \qquad (5)$$

$$OH_{ads} + H^+ + e^- \rightarrow H_2O \qquad (6)$$

Pathway b:

$$O_{2(ads)} + H^+ + e^- \rightarrow OOH_{ads} \qquad (7)$$

$$OOH_{ads} \rightarrow O + OH_{ads} \qquad (8)$$

$$O + H^+ + e^- \rightarrow OH_{ads} \qquad (9)$$

$$OH_{ads} + H^+ + e^- \rightarrow H_2O \qquad (10)$$

$$OOH_{ads} + H^+ + e^- \rightarrow H_2O_2 \qquad (11)$$

$$H_2O_2 \rightarrow 2OH_{ads} \qquad (12)$$

For four-electron mechanisms, as shown in Figure 4 (a), after the oxygen gas is transferred to absorbed oxygen (Eq.(3)), there are two common pathways. One is denoted as O_2-diss-gas[39] (Pathway a): the absorbed O is formed through the O_2 dissociation step (Eq.(4)), then combines with a proton and an electron to produce absorbed OH (Eq.(5)), followed by the reduction with protons and electrons to form H_2O (Eq.(6)).

The other one is called HOO-form-gas[39] (Pathway b): the intermediate superoxide is formed by an oxygen molecule, a proton and an electron (Eq.(7)). After the breaking of the O−O bond, the absorbed O and OH species are produced (Eq.(8)) and then reduced to H_2O by combining with protons and electrons (Eq.(9) and Eq.(10)). Also, the intermediate superoxide combines with a proton and an electron to form hydrogen peroxide, then becomes absorbed OH species by cleavage reaction (Eq.(11) and Eq.(12)).

According to the general ORR mechanism in alkaline solutions proposed by Anastasijevic *et al.*[40] it consists of following steps:

$$O_{2(ads)} + e^- \rightarrow O_2^- \qquad (13)$$

$$O_2^- + H_2O + e^- \rightarrow HO_2^- + OH^- \qquad (14)$$

$$HO_2^- + e^- \rightarrow O^- + OH^- \qquad (15)$$

$$O^- + H_2O + e^- \rightarrow 2OH^- \qquad (16)$$

$$O_{2(ads)} \rightarrow 2O_{(ads)} \quad (17)$$

$$O_{(ads)} + e^- \rightarrow O^- \quad (18)$$

$$O^- + H_2O + e^- \rightarrow 2OH^- \quad (19)$$
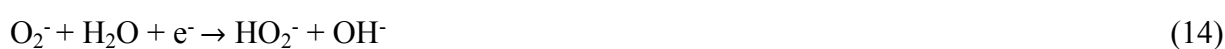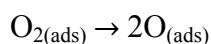
As can be seen from Figure 4 (b), the first step is that the O_2^- is formed by the absorbed oxygen molecule with an electron (Eq.(13)) and the intermediate O_2^- has been detected by surface-enhanced infrared reflection absorption spectroscopy with attenuated total reflection in the ORR in an aqueous solution at pH = 11, as reported by Shao et $al.$[41] Then the formation of species HO_2^- is followed by the reaction of O_2^- with water and an electron, as shown in Eq.(14). Finally, the HO_2^- is further reduced to OH^-, as shown in Eq.(15) and Eq.(16). Another possible pathway is that the absorbed O species are formed by the dissociation of O_2 (Eq.(17)), then these species are reduced to O^- (Eq.(18)), followed by the further reduction to OH^- (Eq.(19)).

According to Kinoshita's work, a four-electron pathway appeared to be predominant for Pd electrocatalysts.[7] However, Kim et al. researched the oxygen reduction on bare Pd in 0.1 M LiOD solution and found that about one third of the O_2 reacts at a bare Pd surface and is reduced directly to OD^- via the four-electron pathway, while the rest are reduced to deuterium peroxide via the two-electron pathway.[42] Therefore, the ORR catalysts are expected to have the optimal balance between both the cleavage and the reduction of the oxygen.

Furthermore, representative studies focused on the ORR process and other possible mechanisms were proposed, such as oxygen hydration mechanism,[43] peroxide mechanism,[44] aquoxyl mechanism,[44] etc. While alloying with various elements, the mechanisms on Pd or Pt alloys for ORR[45-50] are more sophisticated and need further investigation. Advanced characterization techniques need to be applied to understand mechanisms. For example, Wang et al. used shell-isolated nanoparticle-enhanced Raman spectroscopy (SHINERS) to illustrate ORR processes that occur on the surface of bimetallic Pt_3Co nanocatalyst structures.[49] They found the direct spectroscopic evidence of *OOH, which suggests that the ORR undergoes an associative mechanism on Pt_3Co in both acidic and alkaline media.

With the aid of DFT calculations to study the ORR mechanism, there were more attempts in the field of Pt-based catalysts to study the ORR mechanism,[50-55] and relatively fewer studies for Pd-based catalysts.[55, 56] Except for the similarities between the two, there are differences on ORR mechanisms for Pd and Pt electrocatalysts. For instance, the enthalpies and barriers for

each step are different and the ORR process varies under specific conditions. For example, Ford *et al.* indicted that while the activation barriers for O–O bond scission steps differ by *ca*. 0.1 eV on Pd and Pt, the hydrogenation steps (including $O_2 + H$ and $OH + H$) are kinetically less active on Pd than on Pt, suggesting that overall Pd is less effective than Pt.[44] Sha *et al.* considered that under conditions with high H_{ad}, another mechanism producing HOOH is possible, but this is unlikely under ordinary operating fuel cell conditions.[43] Additionally, Ou *et al.* pointed out that in the presence of hydrated protons, the mechanism of ORR on the Pd(111) surface only involved the O_2 molecule dissociation mechanism, whereas the mechanism of ORR on the Pt(111) surface involved the dissociation mechanism of both O_2 molecule and OOH species.[55] As for the entire four-electron ORR, the protonation of adsorbed O atom to form OH was the slowest step, and it was thus the rate-determining step (rds) for both the Pd(111) or Pt(111) surfaces. Such an rds finding of ORR explained Pt- and Pd-based electrocatalysts showing weaker bonding with atomic oxygen had higher ORR activities.

In addition, there is relatively limited research focusing on the ORR conducted in neutral media (pH = 7).[57, 58] However, microbial fuel cells (MFCs) operated at neutral conditions show promising application prospects. The low concentrations (10^{-7} M) of H^+ and OH^- have negative effects on the ORR kinetics, resulting in high overpotentials.[59] Precious metal catalysts (Pt and Pd, *etc*.) tend not to be the first choice due to the high cost compared to the low power output produced.[60] More breakthroughs are needed in this field. Hence, the methods to enhance the catalytic activity and the factors affecting the ORR activity are described in detail below.

4. Volcano plots of ORR catalysts

The theoretical description of the electrocatalytic phenomena is extremely challenging. In this regard, the density functional theory (DFT) calculations have been extensively used to correlate the ORR activity with certain parameters of the electrocatalysts. The experimental evidence suggests that the ORR activity is related to the strength of the metal-oxygen (M−O) bond, which corresponds to an adsorbed oxygen atom as the ORR intermediate.[61] Metals with very negative oxygen binding energy easily cleave the molecular oxygen but subsequently form strong inert oxides and have an inappropriate cathode potential. Metals with very positive oxygen binding energy, for example, noble metals such as Au and Ag, have a high barrier for

the dissociative adsorption of oxygen, so they also tend to be poor ORR catalysts.[62] With the deepening of our understanding in this area, researchers have linked the physical quantities representing the ORR activity of catalysts with some other factors and represent findings in so-called volcano plots. The development of volcano plots of ORR activity against various factors is shown in Figure 5. It is noted that these factors, including d-band vacancy value, the incipient −O or −OH adsorption potential, the oxygen binding energy, the d-band center, the degree of alloying of the electrocatalysts and the adsorption strength for certain surface reactions, can account for various ORR catalytic performances. All these factors influence each other in determining the best conditions for efficient catalytic behavior for ORR and therefore, it can be noted that better catalytic activity can be achieved under the optimal conditions of these factors.
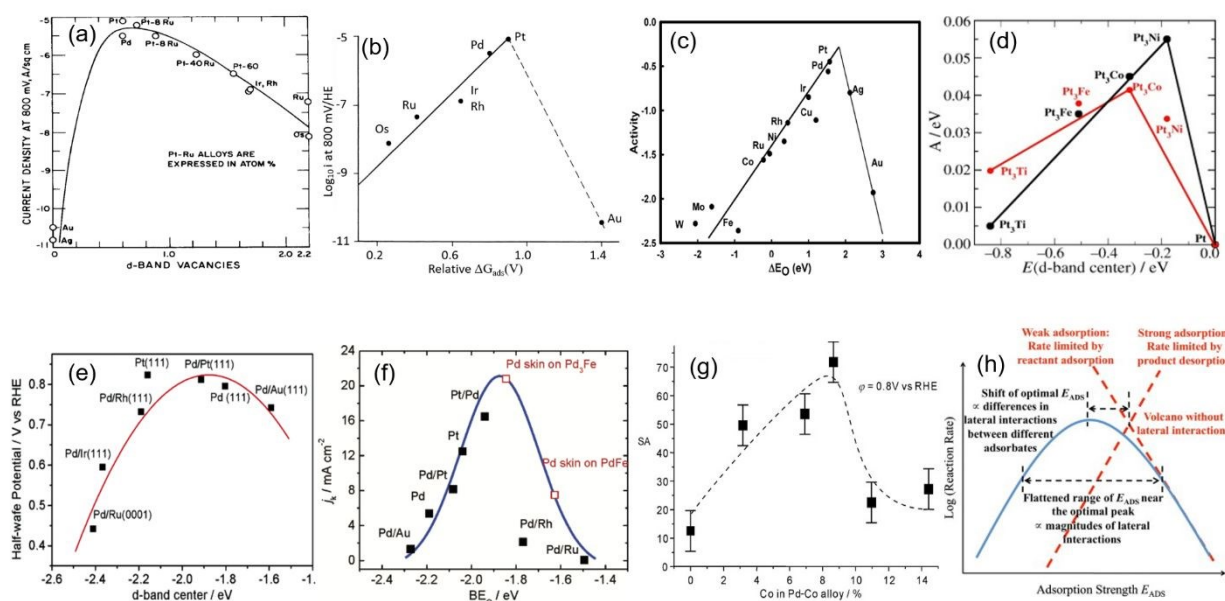
Figure 5. Volcano plots of ORR activity *vs.* various elements. (a) O_2 reduction in 85% orthophosphoric acid: the plot of current density at q = −460 mV at 25 °C against the d-orbital vacancy value of the electrode metal. Reproduced with permission.[63] Copyright 1971, Taylor & Francis. (b) Volcano plots of current density i in ORR *vs.* relative ΔG_{ads}. Reproduced with permission.[37] Copyright 1983, Springer. (c) Trends in ORR activity plotted as a function of the oxygen binding energy. Reproduced with permission.[61] Copyright 2004, American Chemical Society. (d) The volcano plot of ORR activity *vs.* the experimentally measured d-band center. Reproduced with permission.[64] Copyright 2006, Wiley-VCH. (e) The volcano plot of the half-wave potential of Pd-based alloys as a function of the calculated Pd d-band center (relative to the Fermi level). Reproduced with permission.[65] Copyright 2006, American Chemical Society. (f) Volcano plots of the ORR activity (expressed as the kinetic current

density) *vs.* the calculated oxygen-binding energy. Reproduced with permission.[66] Copyright 2007, American Chemical Society. (g) The volcano-type relationship between the surface-specific activity (SA) of Pd–Co alloys and the degree of alloying. Reproduced with permission.[67] Copyright 2007, Wiley-VCH. (h) The relationship between the catalytic activity and the adsorption strength for certain surface reactions. Reproduced with permission.[68] Copyright 2012, Elsevier.

In the 1970s, Appleby showed a volcano plot of the current density, *i*, in ORR *vs.* *d*-band vacancy values of the electrode metal.[63] Pt, Pd and PtRu alloys were at the peak position of this curve, as shown in Figure 5 (a). In 1983, Tarasevich *et al.* demonstrated the volcano plots of the current density, *i*, in ORR *vs.* the relative $\Delta G_{ads}(V)$ (Figure 5 (b)).[37] ΔG_{ads} is the incipient −O or −OH adsorption potential from the anodic cyclic voltammetry. These similar volcano relationships can also be observed in the overpotential η-ΔG_{ads} plots at constant *i* for ORR in the acid solution for platinum group metals, Ag, Au and their alloys. In 2004, Nørskov *et al.* presented a method for calculating the stability of reaction intermediates of electrochemical processes based on electronic structure calculations.[61] Trends in ORR were plotted as a function of the oxygen binding energy. As shown in Figure 5 (c), in terms of pure metal, Pt has the best activity towards ORR and Pd occupies the second place. The model explained the reason that Pt is the best elemental cathode material and the alloying can be used to improve the activity of Pd.

Later, Stamenkovic *et al.* studied the Pt-metal system in detail and described that the variations in the electronic structure determine the trends in the catalytic activity of the ORR across the periodic table.[64] The authors showed that Pt alloys involving 3*d* metals (such as Ti, V, Fe, Co, Ni) are better catalysts than pure Pt because the electronic structure of the Pt atoms on the surface of these alloys has been modified slightly. At first, the catalytic activity is related to the adsorption energy of oxygen ΔE_O. The ΔE_O should be moderate, not be too high or too low (the Sabatier principle). It is well-established in a number of studies that surface bond energies correlate with the average energy of the *d*-states on the surface atoms to which the adsorbate binds (the *d*-band center).[69-73] It is difficult to measure the oxygen bond energy; however, the *d*-band center can be accessible by experiments such as the synchrotron-based high-resolution photoemission spectroscopy[74]. The measurement of the *d*-band center provides a powerful tool to directly correlate the variations in the ORR activity with the changes of the surface electronic structure. As shown in Figure 5 (d), the activity predicted from DFT simulations is shown in

black, and the measured activity is shown in red. Although there is a certain deviation between the two, the overall trend is generally consistent.

Shao *et al.* reported a volcano-type dependence of activity on the energy of the d-band center of Pd monolayers, with Pd/Pt (111) at the top of the curve by using DFT calculation, as presented in Figure 5 (e).[65] Authors considered that due to the strong surface segregation of Pd at high temperature, the downward shift of the d-band center of the Pd that constituted the alloy surface could lead to the high ORR activity. Later, Shao *et al.* established the volcano-type dependence of ORR activity on the binding energy of oxygen (Figure 5 (f)) by combining the experimental data and DFT calculations, and predicted that the Pd overlayer on a Pd_3Fe (111) alloy might have the most active performance.[66]

In 2007, Suo *et al.* described the "volcano" relationship between the ORR activity and the degree of alloying, shown in Figure 5 (g), and noted that the catalytic activity correlates with the adsorption energy ΔE_O, which in turn depends on the lattice strain due to the alloying.[67] In 2012, Qi *et al.* proposed a flattened Sabatier volcano plot in the reduction of oxygen as a result of the adsorbate interactions on surfaces, as shown in Figure 5 (h).[68] Dashed lines are based on a simple Arrhenius relation; the solid line is obtained with the consideration of lateral interactions between adsorbed reaction intermediates. The finite interactions between different reaction intermediates may also shift the optimal adsorption energy and the corresponding maximum activity.
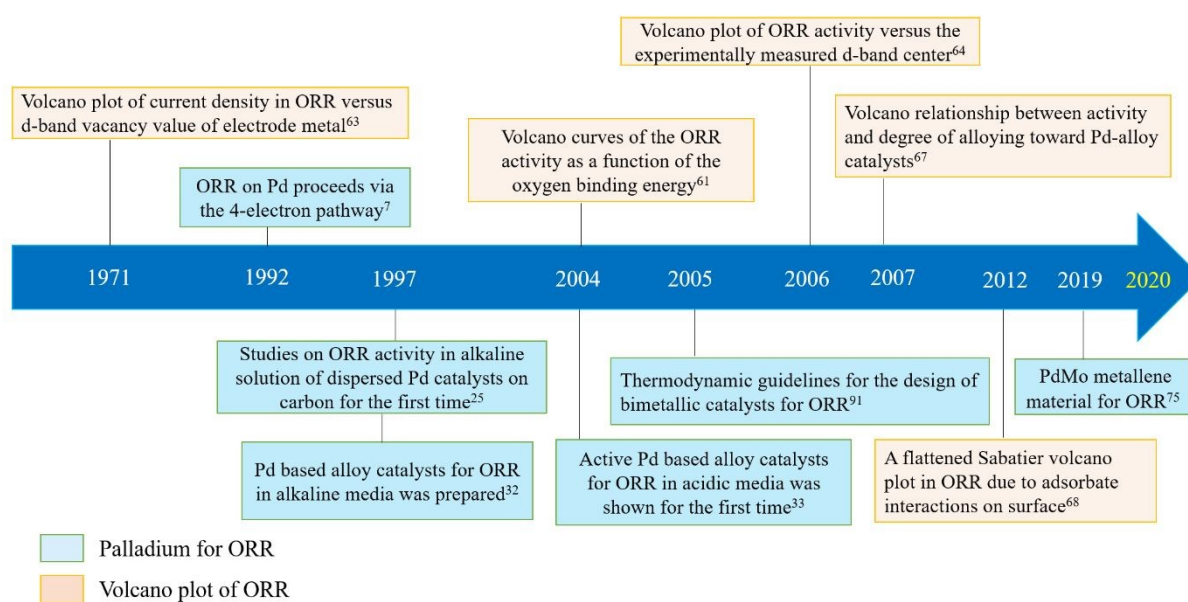
Figure 6. A timeline of palladium(alloys) for ORR and volcano plots towards ORR activity developments.

In Figure 6, the development of volcano plots and their use to understand the ORR activity and the breakthroughs on the application of Pd(alloys) for ORR are presented, which clearly show that the combination of theories and experiments has greatly contributed to the rapid development of this field in recent years. Since 1997, when dispersed Pd-based catalysts on carbon for ORR in alkaline media were first reported,[32] there have been increasing numbers of novel Pd alloys with superior catalytic performance. From realizing the comparable performance with Pt to far exceeding Pt towards ORR performances[75], the research of Pd-based catalysts is constantly delivering breakthroughs. It is believed that Pd-based catalysts could deliver greater achievements in the near future.

5. Methods to enhance ORR activities

There are many factors that contribute to the enhancement of ORR activity. In this section, commonly used methods to enhance the ORR performance are concluded.

5.1 Alloying

There is a growing recognition of enhancing ORR performances by the effect of the alloying process. The ORR activity of Pd can be dramatically enhanced by alloying with other metals, such as Pt,[76] Co,[33] Fe,[36] Cr,[77] Ni,[78] Rh,[79] Ag,[80] Au,[81] Cu,[82] Mo,[75] Ti,[83] Sn,[84] Y,[85] Mn,[86] W,[87] Zn,[88] Ru[89] and Ir.[90]

Fernundez *et al.* proposed a simple thermodynamic model to interpret the enhanced activity on alloying.[91] This model involves the combination of one metal that will easily break the O−O bond of O_2 (forming adsorbed atomic oxygen) with another metal that will easily reduce the adsorbed atomic oxygen. The analysis of the Gibbs free energies of these two reactions guides the selection of combinations of metals that can produce alloy surfaces with enhanced activity for the ORR. In their experiment, PdCo/C (10−30% Co) electrodes exhibited remarkable activities for ORR, close to that of the carbon-supported Pt. For Pd with fully occupied valence *d*-orbitals, Balbuena *et al.* argued that alloying with transition metals, such as Co with unoccupied valence *d*-orbitals, reduced significantly the Gibbs free energy of both the first charge-transfer step, and the steps involving the reduction of intermediates.[92]

In addition, intrinsic Pd surfaces bind oxygen too firmly to allow the efficient removal of the adsorbed reaction intermediates, which affects the ORR activity. For example, in Adzic *et al.*'s work, the volcano-type dependence of the ORR activity on the binding energy of the oxygen and the *d*-band center of the noble metal overlayers was established.[66] They noted that alloying Pd with some transition metals could lower the *d*-band position of the noble-metal overlayers and therefore may improve the activity significantly by inducing strain and electron redistribution between the substrates and the overlayers. Henkelman *et al.* investigated the effect of alloy composition in Pd/Cu nanoparticles on the ORR activity.[93] The activity enhancement is due to the difference in how the two metals respond to a shift in their *d*-band centers. For instance, a charge transfer from Cu to Pd raises the *d* band of Cu and lowers that of the Pd, resulting in a stronger binding between oxygen and Cu and a weaker binding between oxygen and Pd. Henkelman *et al.* also pointed out that the charge redistribution between core and shell in Pd-based core-shell nanoparticles, which became an important factor for lowering the *d*-band center to promote the oxygen reduction.[94] Moreover, the binding energy of the dissociated O_2 molecule is linearly related to the average *d*-band energy of electrons in the Pd shell. Onana *et al.* argued that the enhancement of PdCu alloys was attributed to an optimal d band property that makes easier the OOH dissociative adsorption.[95] Recently, Crooks and co-workers also demonstrated that the activity of the individual sites on the surface of the nanoparticles can influence the overall activity.[96, 97] For example, alloying Pd with Au weakens the O-binding energy on $Au_xPd_{(300-x)}$ alloys, which results in increased ORR activity but in $Pd_xIr_{(100-x)}$ the effect is opposite as O-binding energy increases at the active sites containing Ir.[96, 97]

Additionally, Ou revealed that an ideal Pd-based bimetallic alloy catalyst for ORR should possess simultaneously negative alloy formation energy and negative surface segregation energy of Pd.[98] The alloy formation energy of Pd with transition metals M can be mainly determined by their electron interaction, which could be the origin of the negative alloy formation energy for Pd-M alloys. The surface segregation energy of Pd is primarily determined by the surface energy and the atomic radius of M. The M with a smaller atomic radius and higher surface energy would tend to favour the surface segregation of Pd in corresponding Pd-M alloys.

Furthermore, recent studies found that ORR activity was related to transition-metal dissolution. For example, Han *et al.* found that the amount of transition-metal dissolution from PtM (Pt-

metal) nanoparticles increases when Pt is alloyed with more negative $V_{dissolve}$ transition metals despite their strong alloy-formation energy, where $V_{dissolve}$ or dissolution potential is the thermodynamic potential of the dissolution of transition-metal (M $\Leftrightarrow$ M^{n+} + ne$^-$) at pH = 0.[99] Moreover, the increase of transition-metal dissolution and the decrease of $V_{dissolve}$ were correlated with the ORR activity of PtM nanoparticles. Among all PtM nanoparticles examined, PtFe nanoparticles were found to have the highest ORR specific activities, roughly three times better than that of Pt nanoparticles before voltage cycling. Similar to PtM, PdM is expected to have an analogous effect.

5.2 Structure, strain and ligand

Many studies describe the role of structures and morphologies of electrocatalysts on the enhancement of the ORR. There have been many efforts to manipulate the structure and shape of the catalysts during the synthetic process to fabricate metallic nanoparticles. The structure or shape-controlled metallic catalysts have exhibited improved electrochemical activities because of the exposure of a particular surface, which is favourable for electrocatalytic reactions. Hong *et al.* synthesized PdPt alloy nanocrystals (NCs) with hollow structures such as nanocages with porous walls and dendritic hollow structures.[76] They found that the type of surface facet plays a crucial role in determining the ORR activities of PdPt NCs. The PdPt nanocages prepared from octahedral Pd NC templates exhibited the largest improvement for ORR performance. Duan *et al.* prepared nanoporous PdCr alloys with uniform ligament dimensions and controllable bimetallic ratio.[77] Specifically, the nanoporous Pd$_{75}$Cr$_{25}$ alloy displayed the highest specific kinetic activity with the value of ~0.24 mA cm^{-2} at 0.9 V, which is more than three times higher than that of Pd, and also higher than those of Pt/C (0.15 mA cm^{-2}) catalysts. The Pd$_{75}$Cr$_{25}$ alloy exhibited higher mass activity (0.16 A mg^{-1}), which was nearly 1.4 times that of Pt/C, and 3.1 times that of nanoporous Pd. The improved overall ORR performances of the PdCr alloy could be ascribed to its excellent structural integrity and continuity as well as the appropriate changes in the Pd electronic structure induced by alloying with Cr. By DFT calculations, the authors clarified the reasons for the enhanced ORR performance. The decrease of electron back-donation from the Pd 4d orbital to the 2p* orbital of O usually results in the downshift of the d-band center of Pd, generating a weaker metal–O bond, which was proposed to be the possible cause for the higher ORR activity of PdCr alloys than Pt/C and Pd catalysts.[100, 101]

Core-shell nanoparticles often exhibit improved catalytic properties due to the lattice strain created in these core-shell particles and the substrate material provides an additional advantageous modification of the electronic structures of surface atoms. Chen *et al.* reported the synthesis of bimetallic PdAu nanoparticles with a core-shell construction.[102] The sufficient lattice strain imposed by the Au core and Ag removal, which could tailor the d-band center of the Pd shell, accounting for the enhanced ORR performance of core-shell Au@Pd nanoparticles. Also, Suo, *et al.* noted that the key to improving Pd-based catalysts for ORR is alloying Pd with elements of smaller atomic size to form a "Pd-shell/alloy-core" structure to take advantage of the lattice-strain effect and to prevent the disadvantageous surface-ligand effect.[67]

Xiong *et al.* also studied the surface structure and the strain in PdPt core-shell nanocrystals.[103] From a geometrical phase analysis, they found most of the Pt shells in the icosahedral Pd@Pt nanocrystals are dominated by the compressive strain at a specific size, while, the compressive and tensile strains co-exist in the Pt shells of the octahedral Pd@Pt nanocrystals, which might be responsible for their different ORR properties. Furthermore, Yang *et al.* recently prepared three bimetallic PdZn nanoparticles for ORR and found that the catalytic performance followed the order of Pd@Zn_Core-shell > PdZn_Ordered ≫ PdZn_Disordered, which can be attributed to the effects of different surface structures of the catalysts.[88] Firstly, from the structural perspective, the well-defined core-shell structure and ordered structure can provide more predictable control over geometric and structural effects for catalysis optimization. Secondly, stronger electronic interaction exists in Pd@Zn_Core-shell over PdZn_Ordered and over PdZn_Disordered. Such electronic interaction could make the d-band center of Pd downshift, weakening the adsorption of the oxygenated intermediates.

He *et al.* prepared AuM (M = Pt/Pd) alloyed flowerlike-assembly nanochains (FANs) for enhanced ORR.[104] The authors discovered that the enhanced performances of AuM FANs are mainly ascribed to the interconnected porous bimetallic-alloyed structures, which provide an enlarged electrochemical surface area (ECSAs) and more available active sites for ORR, promote O_2 diffusion and electron transport, and suppress Ostwald ripening. Furthermore, the highly ordered structures and tight interconnection of AuM FANs facilitate the mass transportation of reactant molecules and increase the electrochemically utilized Pt/Pd atoms.

Conformal deposition of Pt as ultrathin shells on facet-controlled Pd nanocrystals offers a great opportunity to enhance the catalytic performance while reducing its mass loading. Wang *et al.* proposed such a system by depositing the active metal as shells of only a few atomic layers on the nanocrystals made of another metal, together with an optimized surface structure.[105] Owing to lateral confinement imposed by twin boundaries and thus vertical relaxation only, the platinum overlayers evolve into a corrugated structure under the compressive strain. Brandiele *et al.* described the facile synthesis of Pd_3Y alloy nanoparticles and confirmed that a strong ligand effect due to the introduction of Y in the Pd lattice affords better catalytic activity through electrochemical characterization.[85] Wang *et al.* describe a facile method for the preparation of Pd-rich Pd_xCo alloy nanoparticles supported on carbon, using an adsorbate-induced surface segregation effect.[106] The electronic properties of Pd were modulated by alloying with different amounts of Co, which affects the ORR activity. Xiao *et al.*'s work offered compelling evidence that surface strain in Pd-based alloyed nanoparticles can be readily tuned by adding Co and Fe elements to achieve optimal electrocatalytic performance.[107] Moreover, Ham *et al.* presented that the electrochemical activity of Pd_3Co alloy catalysts towards ORR can be enhanced by adding a small amount of Ir.[90] Their study highlighted that the enhancing effect is attributed to the synergetic interplay between the surface electronic structure modification due to underlying Ir atoms and the compressive strain caused by the Pd_3Co substrate. The DFT calculations showed that the PdIrCo ternary alloying leads to a noticeable reduction in the DOS peak intensity near the Fermi level and a downshift in the *d*-valence band center, compared to the monometallic Pd (111) surface. They further noted that the addition of Ir to the Pd_3Co alloys causes a slight increase in the activation energy for O−O bond breaking but it significantly decreases for the O and OH hydrogenation, leading to an improved ORR activity. ORR activities of typical Pd-based electrocatalysts with different structures mentioned in this section are compared in Table 2.

Table 2. The summary of ORR activities of Pd-based catalysts measured using the rotating disk electrode (RDE) method at 1600 rpm at room temperature.

Materials	Mass activity (mA mg$^{-1}_{PGM}$)	Specific activity (μA cm$^{-2}_{PGM}$)	Half-wave potential E$_{1/2}$ (V *vs*. RHE)	ECSA (m^2 g^{-1})	Measured potential (V *vs*. RHE)	Electrolyte
PdPt nanocages[76]	764.7	N/A	N/A	40.3	0.85	0.1M HClO$_4$
Pd$_{75}$Cr$_{25}$ alloys[77]	160	240	N/A	N/A	0.90	0.1M HClO$_4$
Pd@Pt icosahedra[103]	3490 [a]	3020 [b]	N/A	N/A	0.90	0.1M HClO$_4$
Pd@Zn core-shell[88]	44.05	48.83	0.82	90.22	0.85	0.1M KOH
AuPd FANs[104]	142.21	480	N/A	N/A	0.90	0.1M KOH
PdY NPs[85]	146	575	0.851	24.83	0.90	0.1M H$_2$SO$_4$
PdY NPs[85]	213	174	0.883	24	0.90	0.1M KOH
Pd$_2$FeCO@Pt/C[107]	2500 [a]	128 [b]	N/A	N/A	0.90	0.1M HClO$_4$

[a] mA mg^{-1} $_{Pt.}$

[b] μA cm^{-2} $_{Pt}$

5.3 Particle size, crystal facet

The particle size of catalysts is also a complicated element in determining ORR activity and many studies focused on the relationship between the size of Pd nanomaterials and catalytic performance. For example, Zhou *et al.* noted that Pd nanoparticle size has a strong impact on ORR in acidic solutions and an optimal average Pd particle size is in the range from 5.0 to 6.0 nm.[108] While in alkaline solutions, Jiang *et al.* conducted similar studies and pointed out that the ORR activity of the catalysts varies with the Pd particle size and the carbon-supported Pd catalysts with the average Pd particle sizes from 3 to 16.7 nm are highly active for ORR.[109] It is noted that the stronger adsorption of OH on smaller particles would block the active reaction sites, so the particle sizes are not as small as possible.

In regards to the particle size effect of PdM alloys, the number of related studies is relatively limited. Castegnaro *et al.* revealed that in alkaline electrolyte, the bimetallic nanoparticles consist of highly crystalline nanoalloys with the size of about 5 nm, where the charge transfer involving Pd and M atoms affects the activity of the catalysts.[110] Furthermore, they noted that different compositions may induce different valence band structure and the materials whose *d*-band center is closer to the Fermi level will have a higher ORR activity.

Crystal facets are also crucial aspects, since relevant research found that the ORR activity depends strongly on the orientation of the Pd surface.[10] For instance, Kondo *et al.* studied catalytic behaviours for ORR in acidic electrolytes on the low index planes, n(100) − (111) and n(100) − (110) series of the Pd and concluded that (100) lattice plane is a possible active site for Pd and ORR activity does not depend on the step structure.[111] Specifically, The specific activity has the following order on the low index planes of single crystal Pd at 0.90 V *vs.* RHE in 0.1 M HClO$_4$: Pd(110) < Pd(111) < Pd(100). This order is completely opposite to that of Pt in 0.1 M HClO$_4$: Pt(100) < Pt(111) $\leq$ Pt(110). Later, Hitotsuyanagi *et al.* extended the study to the ORR on stepped surfaces of n(111) − (100) series of Pd in HClO$_4$ and revealed that the activity increases with increasing terrace atom densities, showing that (111) terrace is the active site for the ORR on n(111) − (100) series of Pd.[112]

In contradiction to the above results, the high catalytic activity of Pd nanorods as compared to spherical Pd nanoparticles has been attributed to the prevalence of Pd (110) facets.[113] Related oxygen reduction studies on Pd nanocubes with a preferential (100) surface orientation have been published.[114, 115] For example, Shao *et al*. indicated that the ORR activity of Pd nanocubes enclosed by (100) facets was one order of magnitude higher than that of Pd octahedra enriched with (111) facets.[114] They have demonstrated that the ORR activity was strongly dependent on the surface structure of Pd nanocatalysts with the exposed (100) facets being much more active than (111) facets.

5.4 Dealloying

Dealloying has generally been known as the selective removal of a less noble component for a given bimetallic alloy. Dealloying is an effective and crucial strategy to control and modify the surface electronic structure and the chemical composition of an alloyed electrocatalyst, thus enhancing activity and stability. Much of the related research has been focused on Pt-based catalysts synthesized by dealloying towards ORR.[116, 117] For Pd based catalysts, relatively limited investigations have been conducted. These Pd based ORR catalysts include PdCo[118], PdCu[119], PdZr[120] and a dealloyed PdAg core Pt monolayer shell electrocatalyst.[121]

Yang *et al*. investigated the ORR activity of electrochemically dealloyed $PdCu_3$ thin films and noted that the ORR activity enhancement is due to the compressive strain in the Pd overlayer in the dealloyed Pd–Cu films.[122] Also, the researchers found that dealloyed structures and the ORR activity are dependent on the nature of the noble component of the alloy. Gunji *et al*. synthesized electrochemically dealloyed $PdCu_3$ intermetallic compound for ORR.[119] They indicated that after electrochemical dealloying, the oxygen binding energy of $PdCu_3$ was lower than that of the Pd (111) structure, and the longer distance between oxygen and the catalyst surface explained the weaker binding of oxygen, which led to the superior ORR activity.

In Lu *et al*.'s research, the electrocatalytic activity was enhanced by the dealloying process, which partially leached out the inactive transition metal species (Mn, Ni) on the surface and generated Pd-rich surfaces on the nanoparticles.[86] The Pd-based dealloyed catalysts exhibited only a slight degradation in ORR activity in alkaline media, which could be reversed by repeating the dealloying process. Mondal *et al*. demonstrated the electrochemical dealloying-assisted Pd-based catalysts

($Co_xCu_yPd_z$) for ORR and indicated that the elemental composition and dealloying-induced lattice strain and the change in the electronic structure due to the downshift in the d-band center of the Pd control the overall performance of the alloy electrocatalysts.[123] However, the dealloying effect of electrocatalysts for ORR can be controversial. Lee *et al.* reported a comparison of alloyed and dealloyed AgPdPt nanoframes for catalyzing ORR and concluded that the mass activity of the ternary catalysts was higher than that of dealloyed ones with less Ag.[124]

Thus, to understand the dealloying effect of PdM, more studies including both experimental and theoretical approaches needs to be conducted. For example, addressing questions on how to conduct systematic research in this area and to provide a general design for these systems are required.

The enhancement for ORR activity can be attributed to many components, like alloying, structure, strain, ligand, particle size, crystal facet and dealloying. Most previous works use theoretical methods to verify their correctness by establishing simple models, and the surface atomic structure of the alloy could be a very important factor for predicting activity. However, bonding between metal atoms may also result in more complicated alloy properties. Catalytic reactions can also take place at surface defects, which is difficult to be simulated and verified. The formation of intermediates (such as hydroxyl) could also dominate the kinetics, or these could bind irreversibly to oxygen cleavage. These factors need to be further examined.

6. PdM (Pd-metal) nanoparticles obtained by different preparation methods

There are many methods reported in the literature to prepare PdM alloys and they could be divided into chemical reduction reaction, electrochemical method, dealloying and so on. The synthesis methods play a vital role in the morphology of the catalysts, which significantly affects the performance of catalysts. In the following chapter, the preparation methods of PdM nanoparticles for ORR will be discussed detailly.

6.1 Chemical reduction reaction

The chemical reduction method is the most common methods for synthesizing alloys. In general, metal precursors are mixed with surfactants, reducing agents and/or capping agents in a solvent (aqueous phase or organic phase), and by controlling the reaction conditions, the alloy catalysts are prepared.

6.1.1 Hydrogen (H₂)

As one of the most common reducing reagents, hydrogen is cheap, clean and relatively simple to operate. However, considering the nature of H_2, there is a certain degree of operational risk.

Ramanathan *et al.* synthesized Pd₃Ni/C catalysts by co-precipitation method from a mixture of $Pd(NO_3)_2 \cdot 2H_2O$ and $Ni(NO_3)_2 \cdot 6H_2O$ salts in an aqueous solution.[125] Pd–Ni hydroxides were formed by slowly adding sodium hydroxide (NaOH) solution and hydrogen was bubbled as a reducing agent at 80 °C, which was further annealed in a reducing atmosphere (10% H_2 + 90% Ar) to reduce the hydroxides to metallic form at about 300 °C for 2 hours. Similarly, Wang *et al.* prepared PdCu alloys by a reduction reaction in a hydrogen atmosphere.[126] They pointed out that the catalyst with the best ORR performance was the alloy nanoparticles with a Pd–Cu molar ratio of approximately 1:1.

Dai *et al.* reported the PdW alloy catalysts for ORR by reducing palladium(II) chloride and ammonium tungstate with H_2 in a tube furnace.[87] Wherein Pd₁₉W/C had the best catalytic activity for ORR. The mass activity of PdW alloys was two-fold that of Pd/C; however, lower than commercial Pt/C.

In addition, according to recent reports, PdCoMo catalysts,[34] carbon-supported PdPtFe alloys,[127] core−shell Pd−Co@Pd/C nanoparticles,[106] Pd₃M (M = Fe, Ni, Cu, Co) alloys,[128,129] bimetallic Pt surface-enriched PtPd(x) nanoparticles,[130] core–shell fct-PdFe@Pd Nanoparticles[131] were prepared by using H_2 to reduce metal precursors.

6.1.2 Sodium borohydride (NaBH₄)

Sodium borohydride ($NaBH_4$) as the reducing agent is often used in aqueous phase reactions with the advantages of low cost and fast reaction rate. Generally, high temperature or high pressure reaction conditions are not required, therefore, the energy consumption of the preparation is relatively small.

Yang *et al*. synthesized three types of PdZn with different surface architectures by using $NaBH_4$ as the reducing agent.[88] Through the heat treatment under 0.1 MPa Ar/H_2 (10%) atmosphere at 600 °C for 5 h, the disordered PdZn alloys turned to ordered PdZn alloys, and the mass activity(MA) and specific activity(SA) of ordered PdZn were markedly higher than that of disordered PdZn. The core-shell PdZn was also obtained through a slightly different reaction process and had better ORR performance. The TEM images of these disordered PdZn, ordered PdZn and core-shell Pd@Zn are presented in Figure 7 (a-c).

Fernández *et al*. prepared carbon supported PdCoAu electrocatalysts by a reverse microemulsion method using sodium dioctylsulfosuccinate (AOT) as the surfactant, heptane as the oil phase and sodium borohydride as the reducing reagent.[83] Remona *et al*. synthesized PdPt alloys by a microemulsion method using $NaBH_4$ as the reductant at room temperature.[132]
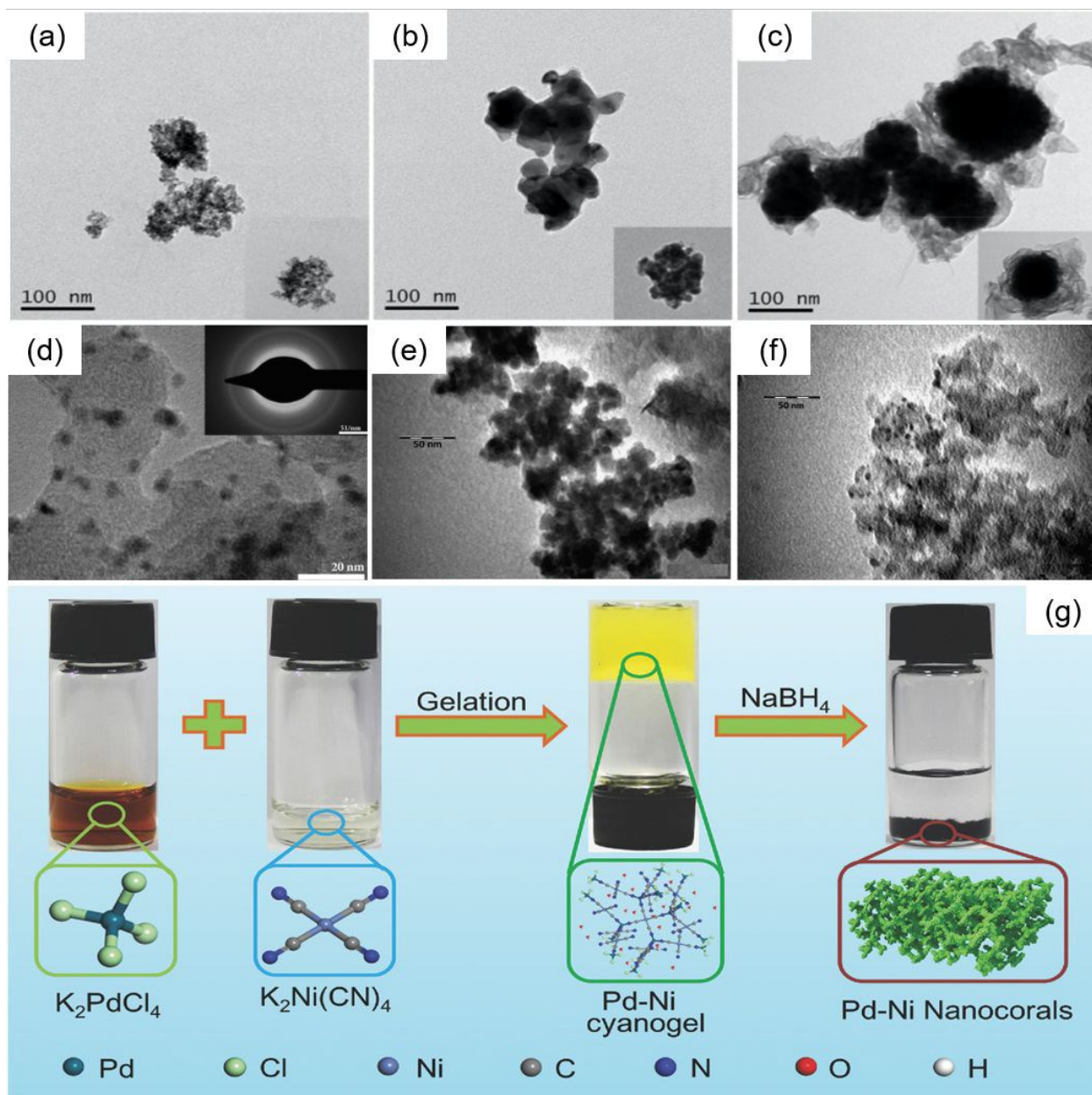
Figure 7. Transmission electron microscope (TEM) images of (a) disordered PdZn, (b) ordered PdZn, (c) core-shell Pd@Zn. Reproduced with permission.[88] Copyright 2020, Elsevier. (d) 20 *wt*.% Pd$_3$Fe/C. Inset shows selected area diffraction patterns of Pd$_3$Fe/C. Reproduced with permission.[12] Copyright 2011, Elsevier. (e) PdNi$_2$/VC, (f) PdNi$_2$/MC. Reproduced with permission.[133] Copyright 2012, Elsevier. (g) Schematic illustration of the synthesis of Pd-Ni nanocorals through a cyanogel-reduction method. Reproduced with permission.[134] Copyright 2018, Wiley-VCH.

Neergat *et al.* prepared carbon-supported PdFe electrocatalysts (Pd to Fe ratios = 1:1, 2:1, 3:1) by co-reduction method at 80 °C in alkaline media (pH = 10) with sodium borohydride ($NaBH_4$) as reducing agents and without any stabilizing agents,[12] as shown in Figure 7 (d). Similarly, Ramos-Sánchez *et al*. reported that the mesoporous carbon-supported nanoparticulated $PdNi_2$ (Figure 7 (e-f)) exhibited higher catalytic activity for ORR, which was synthesized by the reduction of the metal chlorides with $NaBH_4$ in aqueous media.[133]

The preparation of carbon-supported PdCo alloys,[34,135] PdV alloys,[136] PdFe alloys,[12] PdAu nanoparticles[137] also used the $NaBH_4$ reduction method.

Recently, some PdM alloys were fabricated *via* the cyanogel-reduction method with $NaBH_4$ as the reducing agent. The schematic illustration was presented in Figure 7 (g). Firstly, a cyanogel of two metals is formed, and then to reduce with $NaBH_4$. Liu *et al*. reported the preparation of PdNi nanocorals with hierarchical porosity materials through the formation of Pd-Ni cyanogel followed by a chemical reduction with $NaBH_4$ solution.[134] Xu *et al*. prepared polyallylamine (PAA)-functionalized PdCo alloy nanonetworks by functional molecules assisted cyanogel-reduction method using $NaBH_4$/PAA mixture as reductant.[138] The similar strategy was used to prepare the polyethyleneimine (PEI)-functionalized PdNi alloy nanostructures,[139] reduced graphene oxide supported PdNi alloy nanocrystals.[140]

6.1.3 Polyol

Polyol as the reducing agent is often used in solvothermal reactions with the advantages of low-cost and low toxicity. Various polyols are reported to be used in the synthesis of PdM alloys.

Zhao *et al*. reported a polyol reduction method using ethylene glycol as the solvent as well as reducing reagents to synthesize carbon-supported PdNi nanoalloy electrocatalysts.[78] After the heat treatment at 500 °C, the degree of alloying (atomic percentage of Ni in the alloy) was increased from 0 to 13.3%. They found that with increasing heat-treatment temperature (or Ni content), more Ni atoms get into the Pd lattice, resulting in higher lattice strain, weaker M–O_{ads} bonding, and higher specific activity. However, ECSA decreases significantly with temperature, and thus the mass activity shows the volcano relationship with temperature. PdPt catalysts were also synthesized by using a modified polyol process and ethylene glycol (EG) was used as both a

solvent and a reducing agent.[141-143] The similar process was used to synthesize the PdIr alloy networks.[144]

Jang *et al*. presented an ultrasound-assisted polyol process without any added surfactant, pH adjuster, or stabilizer to prepare PdCo nanoparticles with two different structures (core-shell structure and bimetallic alloy nanoparticles, as shown in Figure 8 (a-b).[145] The difference between the preparation methods of the two structures is whether the Co precursor is firstly added to prepare cobalt seeds or Pd and Co precursors are added to the reaction at the same time. The Pd_4Co core-shell structure shows dramatically enhanced ORR activity (its mass activity was 173 mA mg^{-1} and specific activity was about 480 μA cm^{-2}).

In addition, PdM (M = Ni, Fe, Co) nanoparticles were obtained through the reduction of the metal precursors, and 1,2-hexadecanediol was used as a reducing agent and oleic acid and oleylamine as capping agents.[146] Octahedral Pt–Pd nanoparticles were synthesized by reducing metal precursors with the glycerol as a reducing agent and showed good ORR activity in buffer solution.[58]

6.1.4 Ascorbic acid (AA)

Ascorbic acid (AA) is another widely used reductant in the preparation of PdM alloys and is often applied in solvothermal reactions. Besides, Huang *et al.* found that the ascorbic acid not only acts as the reductant but also works as the weak acid to remove the heteroatoms,[147] thus obtaining the catalysts with abundant defects.

Luo *et al*. reported the PdMo bimetallene (Figure 8 (c)) for the reduction of oxygen with the highest mass activity (16.37A mg^{-1}_{PGM}) so far in 0.1 M KOH solution at 0.90 V.[75] This activity was 77.9 and 327.4 times higher than that of commercial Pt/C and Pd/C catalysts, respectively. The value of the specific activity was 11.64 mA cm^{-2}_{PGM}. They used ascorbic acid (AA) to reduce $[Pd(acac)_2]$ and $Mo(CO)_6$ in oleylamine at 80 °C for 12 h to obtain this material. In acid electrolytes, PdMo bimetallene also exhibited better ORR activity than Pt/C, but its stability was poor for practical applications. Zuo *et al*. prepared PdCuCo anisotropic structure catalysts by using ascorbic acid (AA) to reduce metal ions.[148] At 0.8 V *vs*. RHE, the SA of this catalyst could reach 1.61 mA cm^{-2}, and the MA was 1.135 A mg^{-1} in 0.1 M $HClO_4$ solution.

Wang *et al*. prepared PdCuNi nanocrystals (NCs) by reducing palladium acetylacetonate ($[Pd(acac)_2]$), copper acetylacetonate ($[Cu(acac)_2]$), and nickel acetylacetonate ($[Ni(acac)_2]$) in oleylamine (OAm) with ascorbic acid (AA) or benzoic acid (BA) serving as the reducing agents.[149] Through the surface treatment protocol by adding a mixed solution of H_2O_2 and sulfuric acid to remove the surface Ni and Cu atoms, the treated catalysts (PdCuNi-AB-t/C) exhibited a mass activity of 0.45 A mg^{-1} Pd in alkaline medium at 0.90 V *vs*. RHE. It is noted that before the acid treatment, the MA of the catalysts was 0.10 A mg^{-1} Pd under the same conditions. Besides, different reducing agents resulted in various catalytic activities, the combination of BA and AA was better than sole BA or sole AA in this research. Feng *et al*. prepared PdNi icosahedra (Figure 8 (d)) for ORR with a mass activity of 0.22 A mg^{-1} Pd and a specific activity of 0.66 mA cm^{-2} Pd at 0.9 V *vs*. RHE in 0.1M KOH solution.[150] $Pd(acac)_2$ and $Ni(HCO_2)_2 \cdot 2H_2O$ were used as precursors, ascorbic acid (AA) was selected as a reducing agent, and oleylamine (OAm) and 1-octadecene (ODE) were applied as solvents and stabilizers. PdPt alloy nanodendrites[151] were also prepared by using AA to reduce metal ions. Yan *et al*. reported the synthesis of RhPd alloy nanocrystals for ORR by using an extremely slow injection method [79] (Figure 8 (e-f)). This synthesis involved the simultaneous injection of Na_3RhCl_6 and Na_2PdCl_4 using a syringe pump at a rate of 2 mL h^{-1} into ethylene glycol (EG) with ascorbic acid (AA) and KBr serving as reducing and capping agents, respectively. The Rh_8Pd_{92} alloy octahedra exhibited high mass activity with a value of 0.18 mA μg^{-1} in terms of the equivalent Pt cost.
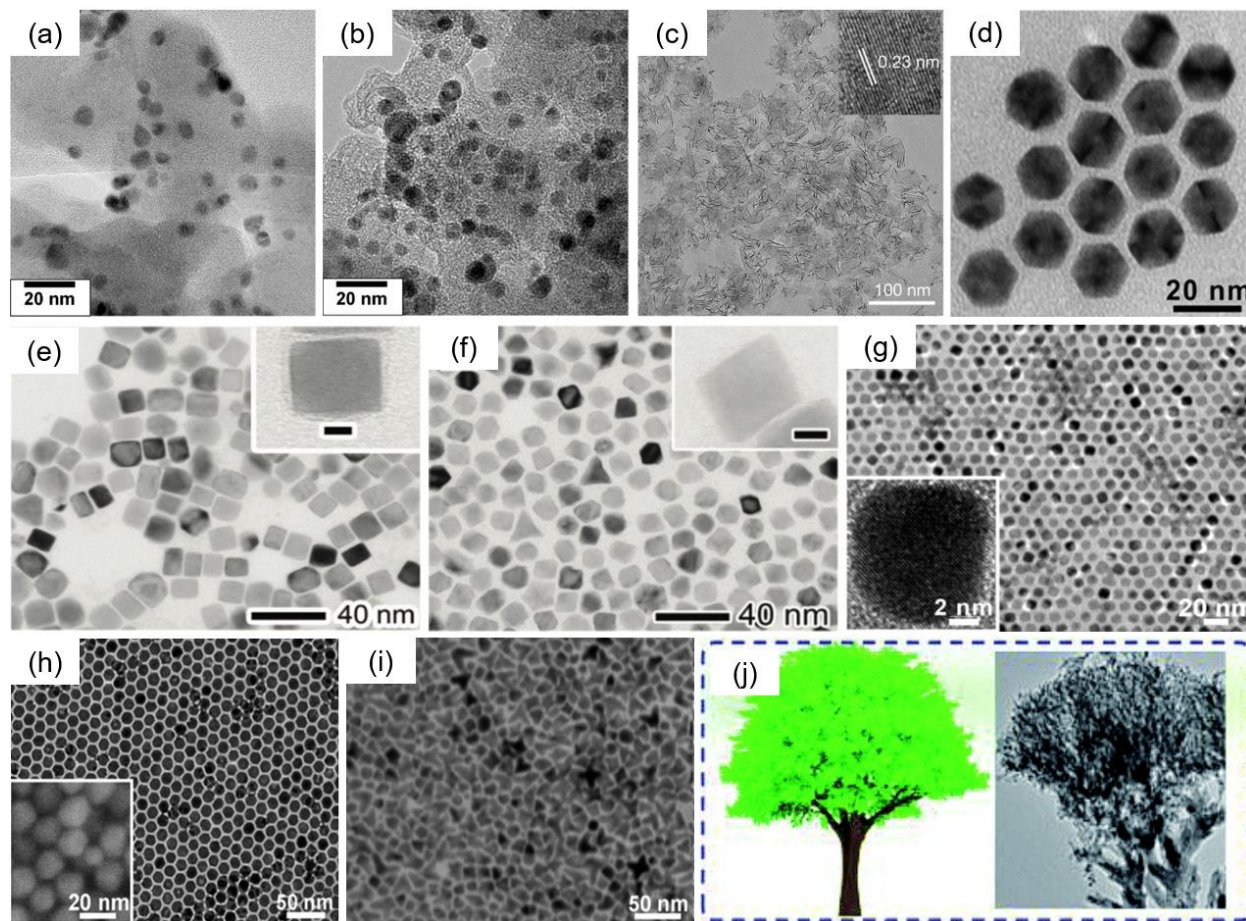
Figure 8. TEM images of (a) as-synthesized $Pd_{80}Ni_{20}$ and $Pd_{80}Ni_{20}$ after heat treatment at (b) 500 °C. Reproduced with permission.[78] Copyright 2010, Elsevier. (c) PdMo bimetallene. Reproduced with permission.[75] Copyright 2019, Springer Nature. (d) Pd_6Ni icosahedra.[150] (e) RhPd alloy cubes and (f) RhPd alloy octahedra. Reproduced with permission.[79] Copyright 2015, Royal Society of Chemistry. (g) truncated cubic, (h) cuboctahedral, and (i) branched (tetrapod-like) CuPd nanocrystals. Reproduced with permission.[152] Copyright 2012, Royal Society of Chemistry. (j) Schematic diagrams and TEM images of the tree-like Pd_3Ag nanocrystals. Reproduced with permission.[153] Copyright 2019, Royal Society of Chemistry. Insets: (c) HRTEM image of PdMo bimetallene; (e, f) TEM images of individual nanocrystals at a higher magnification; (g) HRTEM image of a truncated nanocube and (h) high resolution scanning electron microscopy (HRSEM) image of the cuboctahedra.

6.1.5 Other reducing agents

In addition to the above common reducing agents, other reductants might have excellent and unexpected effects in different synthesis reactions. However, some reagents are expensive, highly

toxic, volatile, and not suitable for mass production. In Zhang *et al.*'s work, a route to fine tailoring of PdCu nanocrystal morphology by controlling the concentration of the reactants was introduced.[152] By reducing copper(II) acetylacetonate ($Cu(acac)_2$) and palladium(II) acetylacetonate ($Pd(acac)_2$) with formanilide in the presence of oleic acid and oleylamine, different PdCu nanocrystals, such as nanocubes, truncated nanocubes, cuboctahedra, irregular polyhedra, and branched tetrapods, could be obtained, as Figure 8 (g-i) demonstrated. Wherein the PdCu nanotubes had the superior catalytic performance with the mass activity (0.130 mA μg^{-1}) and specific activity (0.310 mA cm^{-2}) in acid media. PdPb alloys were prepared by a similar method.[154]

The hierarchical Pd_4Fe nanoflowers (NFs) (Figure 9 (a)) in Lian *et al.*'s work were prepared by reducing palladium acetylacetonate with $Fe(CO)_5$ and oleylamine at 120 °C.[155] The MA of the Pd_4Fe NFs was 521 mA mg^{-1}_{Pd} at 0.85 V, and the SA of this catalyst was 1.57 mA cm^{-2} in a 0.1 M $HClO_4$ aqueous solution. Meanwhile, in a 0.1M KOH aqueous solution at 0.85 V, the MA and SA were 4.07 A mg^{-1}_{Pd} and 11.6 mA cm^{-2}, respectively. Regardless of acidic or alkaline electrolytes, the Pd_4Fe NFs catalyst exhibited excellent catalytic activity towards ORR. Cui *et al.* prepared Pd_3Pb intermetallic compound (Figure 9 (b)) for ORR by a modified impregnation-reduction approach.[156] It included the mixture of Pd and Pb precursors with carbon black in THF, co-reduction of Pd and Pb precursors, and heat treatment. Potassium triethylborohydride (KEt_3BH) and lithium triethylborohydride ($LiEt_3BH$) were used as reducing agents because they both had fast reduction kinetics. The MA of the Pd_3Pb catalysts was 168.9 mA mg^{-1}_{Pd} at 0.9 V in KOH solution. He *et al.* synthesized alloyed PdAu nanochain networks (NCNs) (Figure 9 (c)) by using freshly-prepared hydrazine (80%) to reduce the allantoin solution of $HAuCl_4$ and H_2PdCl_4.[157] At 0.85 V *vs.* RHE in 0.1M KOH solution, the SA and MA of PdAu NCNs were 0.59 mA cm^{-2} Pd and 86.01 mA mg^{-1}, respectively. The presence of allantoin suggested the increased degree of alloying Au with Pd, which was conducive to the improvement of catalytic activity.

Kuai *et al.* prepared PdAu core-shell nanoparticles by using polyvinylpyrrolidone (PVP) to reduce the solution of $HAuCl_4$ and H_2PdCl_4.[158] Moreover, if cetyltrimethylammonium bromide (CTAB) was added, polycrystalline PdAu alloys were prepared. PdPt Popcorn-shaped catalysts were obtained *via* a hydrothermal method involved the co-reduction of K_2PtCl_4 and $PdCl_2$ in an aqueous solution containing PVP and NaI.[159] Authors found that If NaI was absent, octahedrons (≈ 20 nm)

and very small particles ($\approx$ 3 nm) were generated for Pt and Pd. The bio-synthesis of palladium nanocubes (PdNCs) was realised using pine needle extract as the reducing agent and CTAB as the capping agent. As eco-friendly and readily available biomass, pine needle extract avoided the use of highly polluting chemical reducing agents.[160] 1-naphthol ethanol solution as the reductant and structure-directing agent was applied to fabricate the tree-like Pd_xAg_y nanocrystals[153] (as shown in Figure 8 (j)). Chemical reduction reactions can be used to prepare metal alloy catalysts with various morphologies and properties, and a reasonable selection of reducing agents cannot be ignored. However, the reaction temperature ranges from room temperature to several hundred degrees Celsius, and the types of reagents and experimental methods used in the reaction vary greatly. To obtain a catalyst with excellent performance, it is very important to explore the experimental conditions.

6.2 Electrochemical methods

Electrochemical methods are another way to prepare alloys. Compared with traditional chemical reduction methods, electrochemical methods are environmentally friendly without organic reducing agents, surfactants or high temperature, and provide a rapid and effective route to prepare hollow nanostructures. However, to accurately control the structure, these methods often require complicated multistep operations and specific equipment, such as pulsed electrodeposition, which may not be available in many laboratories.

6.2.1 Electron reduction

Electron reduction method does not require chemical reducing agents, protective chemicals or dispersants. Moreover, this method can be used to synthesize alloys with small particle diameters when the precursor is a mixture of different metal salts.[161] Liu *et al.* reported PdPt alloys with a particle size around 2.6 nm for ORR synthesized by electron reduction at room temperature with argon glow discharge as an electron source, and without any chemical reducing agents, protective chemicals nor dispersing agents.[161] The Pt_1Pd_1/C catalyst (Figure 9 (d)) has the larger MA of 0.488 mA μg^{-1}Pt in 0.5 M H_2SO_4 solution at 0.85 V *vs*. RHE. The kinetic current j_k of Pt_1Pd_1/C catalyst was 0.976 mA cm^{-2}. Liu *et al*'s group also prepared PdAu alloys by using this electron reduction method.[162]

6.2.2 Underpotential deposition (UPD) and electrodeposition

Underpotential deposition (UPD) is an electrochemical surface process that involves depositing one (or two) monoatomic layers of metal on the electrode surface with an applied potential that is more positive than its equilibrium potential.[163] This method has been extensively studied over decades and could accurately and reproducibly control the amount of the foreign metal adsorption atoms on the substrate,[164] therefore it is very useful for surface modification with the aim of improving functional properties, such as catalytic activity and selectivity.[165] Electrodeposition has been widely used in the preparation of metal alloys. In contrast to physical deposition methods, it does not require a vacuum environment.[163] Some types of alloys can be hard to prepare by thermal methods but are easier to obtain by electrodeposition, such as an alloy composed of both low-melting volatile constituents and high-melting metals.[166] Electrodeposited alloys have enhanced properties and possess special properties.[166] However, there are limited reports on the application of these methods to prepare Pd alloys for ORR application.

Betancourt *et al*. reported a strategy to prepare PdAg alloys for ORR using a UPD method.[80] They have used underpotentially deposited Cu and subsequent galvanic displacement to deposit atomically dispersed loading of Pd to achieve precise tuning of the electronic properties. The Pd@Ag/C catalysts had a higher normalized Pd mass activity with the value of 878 mA mg^{-1} in 0.1M NaOH at −0.1 V *vs*. Hg|HgO. In addition, Gobal *et al*. synthesized PdCu alloys by electrodeposition method.[167]

6.2.3 Galvanic replacement reaction

Galvanic replacement method provides a one-step and universal route to prepare hollow nanostructures of noble metals (Pd, Pt, Au) on a large scale, and the morphology, void space, and shell thickness of these hollow structures can be controlled by solid templates.[168, 169]

Xu *et al*. prepared nanotubular mesoporous PdCu catalysts through the galvanic replacement reaction using dealloyed nanoporous Cu as both the template and reductant.[170] This material exhibited a half-wave potential of 0.840 V for the ORR, superior to the commercial Pt/C (0.825 V) in 0.1 M HClO$_4$ solution. PdFe@PdPt/C was also prepared by the galvanic replacement reaction between PdFe/C alloy nanoparticles and PtCl$_4^{2-}$.[127]

Energy & Environmental Science Accepted Manuscript

6.2.4   Pulsed electrodeposition (PED)

Pulsed electrodeposition (PED) is an advanced type of electrodeposition. By controlling the interface supply and electrochemical reaction, the deposition performance can be well-controlled,[171] which allows accessing a non-equilibrium synthetic environment, thereby promoting the synthesis of metastable ordered intermetallic nanoparticles.

Wang *et al*. presented the pulsed electrodeposition process to prepare PdBi alloy electrocatalysts for ORR.[172] $Pd_{31}Bi_{12}$ ordered alloys (Figure 9 (e)) grown directly onto the carbon supports by deposition from an aqueous electrolyte containing ethylenediammenetetracetic acid (EDTA), $Bi(C_2H_3O_2)_3$ and $Pd(NO_3)_2$ at 30 °C. The SA and MA of $Pd_{31}Bi_{12}$ were 2.42 ± 0.2 mA cm^{-2}_{Pd} and 0.95 ± 0.18 A mg^{-1}_{Pd} at 0.9 V *vs*. RHE in 0.1M KOH electrolyte.
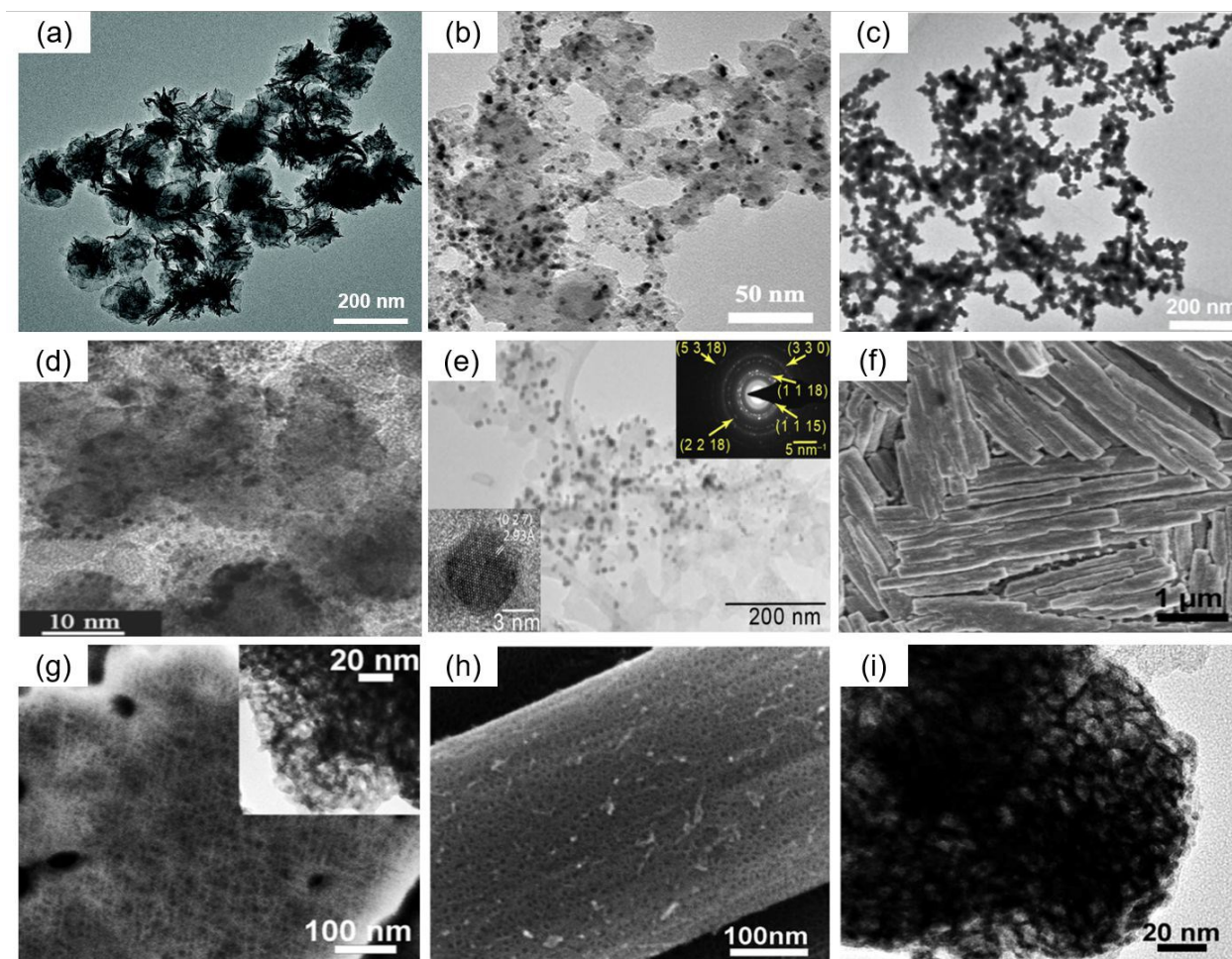
Figure 9. Representative TEM images of (a) Pd_4Fe NFs. Reproduced with permission.[155] Copyright 2018, Royal Society of Chemistry. (b) ordered Pd_3Pb/C. Reproduced with permission.[156] Copyright 2016, American Chemical Society. (c) alloyed PdAu nanochain networks. Reproduced with permission.[157] Copyright 2015, Elsevier. (d) Pt_1Pd_1/C.[161] (e) $Pd_{31}Bi_{12}$/C nanoparticles and corresponding selected area electron diffraction (SAED) pattern. Reproduced with permission.[172] Copyright 2019, American Chemical Society. (f) SEM images of NP-$Pd_{75}Cu_{25}$, (g) alloys by dealloying the source alloys in 0.2 M H_2SO_4 solution for 48 h at room temperature. Inset of (g) is the TEM image of the NP-$Pd_{75}Cu_{25}$. Reproduced with permission.[82] Copyright 2013, Elsevier. SEM (h) and TEM (i) images of the resulted samples by dealloying the PdNiAl alloy in 0.5 M NaOH solution for 48 h at room temperature. Reproduced with permission.[173] Copyright 2013, Royal Society of Chemistry.

6.3 Dealloying

Nanoporous materials obtained by the dealloying method have been proved to represent a particular class of multifunctional catalytic nanoarchitectures with interconnected nanoscale skeletons and voids,[174] which are especially beneficial for electron and mass transport during electrocatalytic processes. The advantages of dealloying are simple and high-yielding preparation methods without any assistance from organic solvents.

6.3.1 Chemical dealloying

Chemical dealloying method generally uses chemical reagents (such as acids and alkalis) to obtain materials with different structures and improved properties.

Zhang *et al.* showed that nanoporous (NP) PdCu alloys (as presented in Figure 9 (f-g)) synthesized by dealloying from ternary PdCuAl source alloys exhibited superior ORR activity and higher catalytic durability compared with Pt/C catalyst.[82] PdCuAl alloy foils were made by refining pure Pd, Cu, and Al at high temperature in an arc furnace, followed by melt-spinning under the Ar atmosphere. The nanoporous metals were prepared by dealloying the alloy foils in 0.2 M H_2SO_4 solution. The mass activity of NP-$Pd_{50}Cu_{50}$ is 0.15 A mg^{-1}_{Pd}, and the specific activity is 0.22 mA cm^{-2}. Similarly, Xu *et al.* presented that NP-PdNi alloys by etching PdNiAl alloy foils in 0.5 M NaOH solution,[173] as exhibited in Figure 9 (h-i). NP-PdNi showed higher specific activity with a value of about 0.21 mA cm^{-2} at 0.9 V and the mass activity of NP-PdNi is about 0.15 A mg^{-1}_{Pd}. PdTi alloys[175] and PdCe[176] were also prepared by a similar method. In Begum *et al.*'s study, Pd nanonetworks (Pd-Net) without any support material were prepared by using 0.1 M HCl etching PdZn alloys.[177] The introduction of CTAB plays a crucial role in the structure and morphology of the catalysts. Pt-Net had higher ECSA and ORR performance than that of commercial Pt/C and homemade Pd nanoparticles in alkaline media.

6.3.2 Electrochemical dealloying

The difference in chemical potential between the elements in the alloys can lead to selective etching of the more active components and it has been regarded as a productive and controllable route to fabricate nanoporous structure.[178, 179] Through the electrochemical dealloying, the structures and compositions of PdM alloys often change, which sometimes can greatly enhance the catalytic activity. However, the electrochemical dealloying method is not favorable for the

control of the bimetallic ratio, which is easily affected by the applied potential and corrosion time, *etc*.

Sun *et al*. reported a process for converting colloidally synthesized ordered intermetallic $PdBi_2$ to ordered intermetallic Pd_3Bi nanoparticles under ambient conditions by electrochemical dealloying to significantly enhance ORR activity,[180] as shown in Figure 10 (a-b). The SA and MA of converted Pd_3Bi were 2.3 ± 0.19 mA cm^{-2}_{Pd} and 1.2 ± 0.08 A mg^{-1}_{Pd} at 0.9 V in alkaline media. Gunji *et al*. synthesized PdM (M = Fe, Co, Ni) alloy catalysts and then electrochemically dealloyed these alloys to enhance the ORR activity.[129] The dealloyed Pd-M nanoparticles had a core-shell structure with a Pd_3M-core and a Pd-shell.

6.4 Other methods

In addition to the above synthesis methods, other methods can also be used for the preparation of PdM alloys. These methods are not widely used in the synthesis of Pd-based alloys, although they are extensively applied in the preparation of other materials, such as carbon materials, other metal nanoparticles (Au,[181] Ag[182]), *etc*. Due to the interoperability of synthetic methods, learning from the preparation of other materials can facilitate the study of Pd-based alloy materials.

6.4.1   Laser-irradiation-induced melting

Laser-irradiation-induced melting is an effective method to prepare bimetallic alloys with tunable size distribution.[183] Brandiele *et al*. reported the process to synthesize Pd_3Y alloy nanoparticles by a robust laser assisted method in pure organic solvents.[85] Laser ablation of the bulk Pd_3Y target was performed with the set up sketched in Figure 10 (c), ethanol, acetone and n-hexane were chosen as the solvents and the obtained PdY alloys had different morphological structures and ORR activities. From TEM images (Figure 10 (d-f)), the large mass of the samples is composed of spherical nanoparticles (NPs) and in the PdY−A and PdY−H samples, a core-shell structure. Among three types of PdY catalysts, PdY−E displayed excellent ORR performance in 0.1 M H_2SO_4 solutions, with the SA (0.575 mA cm^{-2}) and MA (146 A g^{-1}).
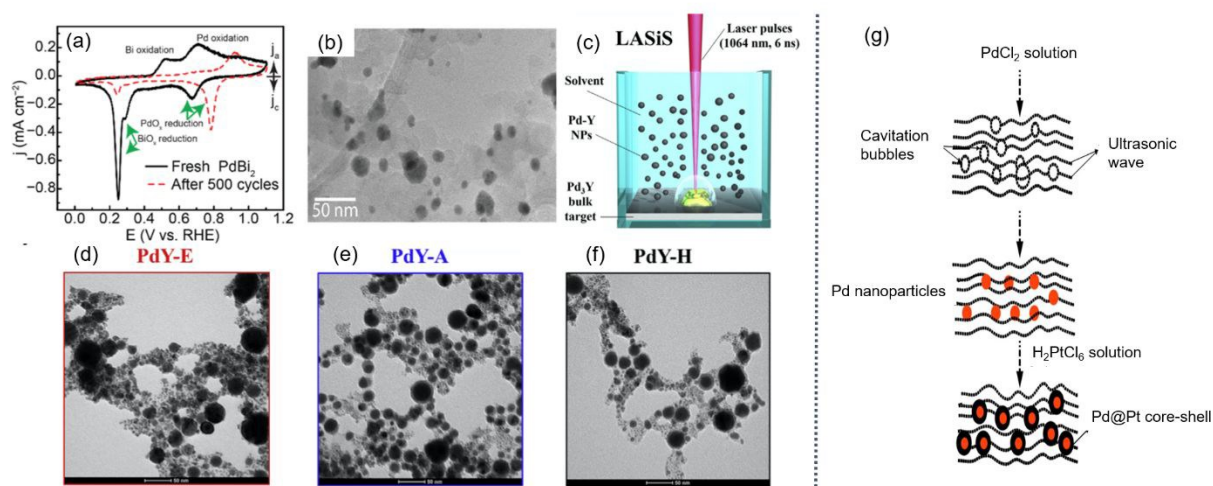
Figure 10. (a) Cyclic voltammograms (CVs) of the PdBi$_2$ in Ar-saturated 0.1 M KOH before and after the electrochemical dealloying; (b) TEM image of dealloyed PdBi$_2$ supported on Vulcan carbon. Reproduced with permission.[180] Copyright 2019, American Chemical Society. (c) Sketch of PdY NPs preparation by laser ablation synthesis in solution (LASiS); Representative TEM images of PdY NPs prepared in (d) ethanol (PdY−E), (e) acetone (PdY−A) and (f) n-hexane (PdY−H). Reproduced with permission.[85] Copyright 2019, Elsevier. (g) Schematic illustration for the synthesis of Pd@Pt core shell using ultrasonication. Reproduced with permission.[184] Copyright 2019, Elsevier.

6.4.2 Sputtering method

The sputtering method has many advantages such as process constancy, dependability, plasma production at low–temperature, high quality and uniform products and industrial practicality with desired chemical composition.[185] Lee *et al*. synthesized PdM alloys (M = Co, Ni, Cr) by an rf sputtering method.[186] The sputtering deposition was made when 1 cm^2 Pd sheets were put on each transition metal target under an argon atmosphere. It is noted that the order of ORR activity of various PdM alloys is different in the presence or absence of methanol. Specifically, in the absence of methanol, the order was Pd–Cr > Pd–Co > Pd–Ni > Pd; while in the presence of methanol, the order was Pd–Ni > Pd–Co > Pd–Cr > Pd. Also, PdCu alloys were prepared by using magnetron sputtering equipment with a Pd and a Cu wafer as targets.[95]

6.4.3 Pyrolysis synthesis

Pyrolysis is a rare way to prepare Pd alloys. It is relatively simple to operate without the addition of surfactants, additives or capping agents. However, it seems difficult to precisely control the morphology and particle size of synthetic materials. Furthermore, it needs high temperatures and the energy consumption is relatively high. PdFe alloys were prepared by thermochemical synthesis.[187] It included the adsorption of solutions of iron and palladium precursors on carbon support, evaporation of solvents and subsequent pyrolysis. It is noted that the presence of basic metal particles (in this case, iron) can depress the agglomeration degree of palladium.

6.4.4 Ultrasonic synthesis

Ultrasonic synthesis offers a simple route to prepare materials by introducing energy into a chemical system through acoustic cavitation from the formation, growth and implosive collapse of bubbles within a liquid.[188] Distinctive properties of noble metal nanoparticles by ultrasonic synthesis have been achieved with a narrower size distribution, larger surface area, and much smaller size.[189] Karuppasamy *et al.* reported the preparation of reduced graphene oxide (rGO) nanosheet-supported PdAg nanoparticles by using a simultaneous ultrasonic probe irradiation method.[189] The mass activity of PdAg (1:1)/rGO alloy was 1.01 mA mg$^{-1}_{Pd}$, the specific activity was 806 μA cm$^{-2}_{Pd}$. Zheng *et al.* prepared Pd@Pt/C core-shell nanoparticles *via* sonochemical synthesis,[184] as Figure 10 (g) demonstrated.
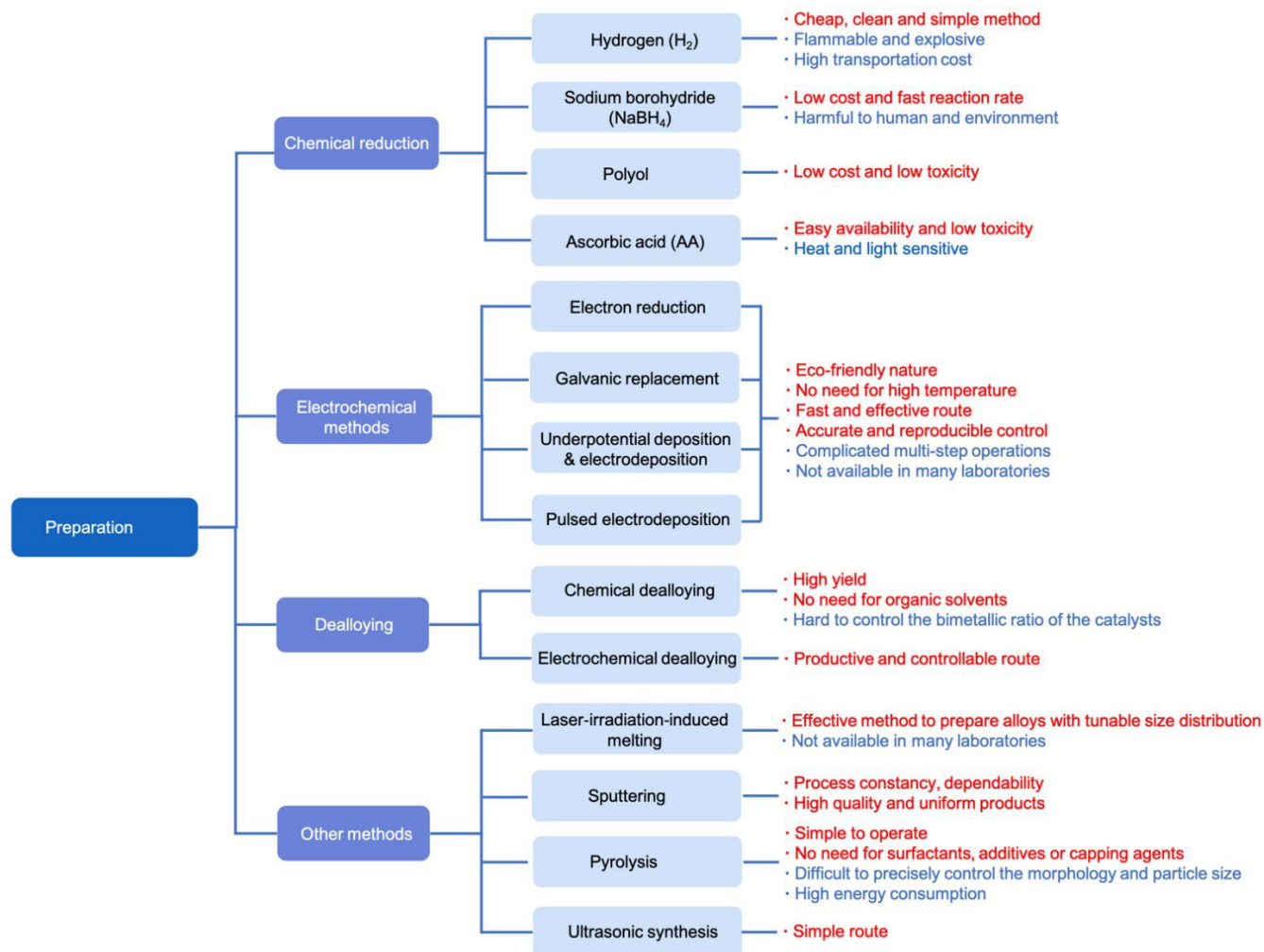
Figure 11. Comparison of different synthetic methods to obtain PdM alloys.

In short, various synthetic methods of PdM alloys are summarized in Figure 11. Among synthetic methods of Pd-based alloys, the most commonly used method is the chemical reduction, while electrochemical methods are regarded as simple and environmentally friendly routes to prepare nanomaterials with a tunable size distribution, chemical composition and desired morphology. Moreover, the number of other methods has gradually increased, and various new methods have also appeared to be used in the synthesis of Pd-based alloys with excellent ORR performance. In addition, during the synthesis of Pd-based alloys, the following concerns need to be noted.

(1) The effect of heat treatment

(a) Change the structure of alloys. In Yang *et al.*'s work, the disordered type is changed to the ordered type *via* the heat treatment, which increases the ORR activity.[88] Also, Maiti *et al.* mentioned that through the high-temperature treatment at ~500 °C in the Ar/H$_2$ atmosphere, phase transformation of the face-centered cubic (fcc) to face-centered tetragonal (fct) of PdFe alloys was achieved, which is due to the movement of core Pd atoms to the surface of the alloy as Pd has higher adsorption enthalpy of H than Fe, resulting in the formation of the fct-PdFe@Pd structures.[131]

(b) For core-shell structure, the heat treatment at a low temperature can facilitate core–shell structure formation which plays a key role in enhancing the ORR activity of PdCo alloy catalysts.[190]

(c) For PdFe, PdCu alloys, annealing at elevated temperatures enabled both Pd enrichment on the surface and an increase in ECSA, thus enhancing the ORR performance.[128]

(d) The degree of alloying can be increased to a certain extent, which is conducive to the improvement of catalytic activity, but the post-treatment temperature should not be too high, which may lead to an increase in particle size and consequent decrease in the electrochemically active surface area.[78, 83, 135, 191] But there are some exceptions, in the case of the Pd$_{60}$V$_{40}$ sample, heat treatment at 300 °C decreased the ORR performance of the as-prepared sample.[136]

(e) Remove the organic reagents (such as surfactants, capping agents, *etc.*)[192]

Therefore, these issues are clearly complicated and further experimental and theoretical work is required to fully understand the effect of heat treatment on electrocatalytic activity.

(2) The effect of CO reagent

Through the comparison of Figure 12, it is noted that CO reagent is used in the synthesis process of many Pd-based alloy catalysts with extremely high catalytic activity, such as PdMo bimetallene[75] and Pd$_4$Fe nanoflowers[155]. Besides, Ahmad *et al.* used W(CO)$_6$ to synthesize W-doped Pd nanocubes.[193] At 0.9 VRHE, the specific activity of 1.2%W-doped Pd nanocubes/C was 1.18 mA cm^{-2}, which surpassed most reported Pd-based catalysts for ORR in alkaline media.

Some researchers have specifically studied the role of CO reagent. For example, Wei *et al*. reported the effect of the CO treatment for PdCoAu catalysts.[194] The authors found that the CO treatment can modify the PdAu and PdCo alloys ratios in the bulk structure and result in the formation of Pd–Au alloy enriched on the outer shell, thereby increasing the ORR performance. The PdCu/C catalysts heat-treated in CO have the ultimately high alloying degree and electrochemical activity towards ethanol oxidation reaction compared with those treated under O_2 and H_2.[195] The CO-confinement effect, which is the strong binding of CO on the metal (111) facets, is used to induce the formation of 2D nanomaterials.[196] Therefore, more in-depth research in this aspect needs to be done.

(3) The effect of solvents

In chemical reactions, the role of solvents is often less noticeable, but its impact cannot be ignored. The solvent will affect the morphology and structure of the Pd-based catalysts.[159] Zheng *et al*. found that during the synthesis of both Pt and Pd nanoparticles using H_2 as the reducing agent at room temperature, ethylene glycol (rather than the commonly used water) was used as the media can minimize the aggregation of particles during their formation due to the high viscosity, thereby controlling the particle size.[130] Also, it is found that the solvent played significant roles in controlling the synthesis of intermetallic Pd_3Pb square nanoplates.[154]

(4) The effect of doping

(a) To improve selectivity

Pd-based alloys also have high catalytic activity for methanol/ethanol oxidation reaction. To avoid the poisoning problem induced by the alcohol crossover effect, achieving the selectivity of Pd-based alloys towards ORR is highly desired. The surface chemical functionalization of metal nanocrystals was used in Pd-based alloys to enhance the ORR selectivity, such as polyallylamine (PAA)-functionalized PdCo alloy nanonetwork.[138]

(b) To improve methanol tolerance

For instance, the essential role of Rh in obtaining high methanol tolerance capacity was reported in Rh-doped PdAg nanoparticles.[192]

(c) To improve ORR activity

The surface decoration induced structural change could directly influence the electronic structure, thereby improving the catalytic activity, such as Pt submonolayer decorated PdAu/C Nanocatalyst.[137] Besides, polyethyleneimine (PEI) as a dopant was reported.[139] Specifically, $-NH_2$ groups on the modified PEI polymer can been protonated into $-NH_3^+$ in an acidic medium, which will increase the interfacial H^+ concentration on the Pd surface and consequently accelerate proton-coupled electrocatalytic reactions (such as the ORR and HER).[197]

(5) The effect of reductants

Calderon *et al.* studied the effect of five different reductants (methanol, ethanol, *n*-propanol, formaldehyde and ascorbic acid) on the ORR activity of PdPt catalysts.[198] Different reductants can tune the size and surface Pt content, thus influencing the properties of catalysts. In addition to several common reducing agents, the introduction of other new reducing agents may bring surprises, such as pine needle extract as the reducing agent,[160] 1-naphthol ethanol solution,[153] urea slowly degraded to NH_3 during pyrolysis[199] and borane tert-butylamine complex.[200]

(6) The effect of additives

The introduction of some additives can affect the morphology and properties of the catalyst, such as EDTA,[158, 177] arginine,[201] glycine,[202] NaI,[159] amines,[196] *etc*.

(7) The effect of carriers

In this review, we did not conduct a detailed analysis of the role of the carriers. But a suitable carrier will greatly enhance the catalytic performance of Pd-based alloy catalysts, such as ordered mesoporous carbon (OMC)[143], defective mesoporous carbon,[203] nitrogen-doped graphene,[199] $CoFe_2O_4$-Vulcan composite,[200] and carbide-derived carbons (TiC, Mo_2C and SiC),[204] *etc*. The issue that carbon-support corrosion leads to a decrease in stability of catalysts is worthy of further investigation.[205]

(8) Other considerations

For Pd-based alloys prepared with different metals M or different synthesis methods, the ratio of Pd to M at the optimal activity is uncertain. For example, the maximum activity for the ORR was

observed at the alloy composition of ~60 atom % Pd for the three types of PdM alloys (M = Co, Ni, Cr).[186] While in Liu *et al.*'s investigation, $Pd_{70}Co_{30}$/C alloys had the highest catalytic activity.[206] As for PdCu alloys, the molar ratio of approximately 1:1 showed the optimal alloy composition.[95, 126] Using a combination of multiple synthesis methods to synthesize highly active ORR catalysts is a method to control the structures of targeted materials. For instance, in You *et al.*'s work, three catalysts with PdNi, PdNiCu and PdCu cores and a PdIr shell were fabricated by polyol method and galvanic replacement.[207] Chen *et al.* reported a process to prepare nanoporous PdCe (NP-PdCe) nanocubes by melt spinning combined with chemical dealloying.[176] Carbon supported PdCu alloyed catalysts were prepared by using a two-step process involving the synthesis of Cu nanoparticles, followed by galvanic substitution of Pd on Cu nanoparticles.[208] Focusing on the efficient bifunctional catalysts, for example, PdIr alloys[144] as the efficient bifunctional catalysts for oxygen reduction and oxygen evolution reactions, tree-like PdAg nanocrystals towards the anodic formic acid oxidation and cathodic oxygen reduction[153] were reported. Additionally, Pd alloyed with novel elements is worthy of attention, such as PdTe,[209] PdCe,[176] *etc*.

Finding suitable ORR catalysts used in proton exchange membrane fuel cells (PEMFC) is a key concern, and ideal catalysts should meet the requirements of good reliability, durability and stability in acidic electrolytes.[210] One of the main issues for Pd-based catalysts is the Pd dissolution under operating conditions including low pH, high temperature, high potential and frequent start-stop cycling.[10] Compared with Pt, Pd is much more easily dissolved.

In acid solution, the main pathways for Pd dissolution include direct dissolution (Eq.(20)) or an oxide film formation (Eq.(21)) and a subsequent chemical reaction (Eq. (22)).[211]

$$Pd \rightarrow Pd^{2+} + 2e^- \tag{20}$$
$$Pd + H_2O \rightarrow PdO + 2H^+ + 2e^- \tag{21}$$
$$PdO + 2H^+ \rightarrow Pd^{2+} + H_2O \tag{22}$$

In the direct dissolution pathway, the equilibrium potential of Pd dissolution is 0.2 V lower than that of Pt. In the chemical dissolution pathway, the Pd^{2+} equilibrium concentration is ~5 orders of magnitude higher than that of Pt^{2+}. Thus, Pd is much less stable than Pt in an acid medium.[212]

It is noted that Pd/C was not regarded as an ideal catalyst for ORR in acid solution due to the gradual degradation during potential cycling.[213] However, some Pd-based alloys which had good stability in acid media were reported.[148, 173]

In addition, Ou *et al*. compared the ORR mechanisms on the Pd (111) and Pt (111) surfaces in acidic solution by DFT,[55] and revealed that the adsorption and dissociation processes of O_2 molecule more easily occurred on the Pt (111) surface and that the serial protonation of the dissociative product to form H_2O molecule could also more easily occur on the Pt (111) surface than on the Pd (111) surface, indicating that Pt can serve as a better ORR electrocatalyst than Pd.

In general, Pd-based catalysts are still not comparable to Pt-based ones in terms of ORR activity and stability in acidic electrolytes. More efforts need to be taken to achieve new breakthroughs.

7. Electrochemical analysis

Electrochemical analysis determines the specific performance of electrocatalysts, which is particularly important for Pd-based electrocatalyst optimization. Accordingly, typical methods on the electrochemical analysis, including determination of electron transfer number (n) and electrochemically active surface area (ECSA), durability evaluation protocols and standardization on electrochemical analysis process are concluded in this section, as well as the performance of representative Pd-based ORR electrocatalysts.

7.1 Electron transfer number (n)

The electron transfer number per O_2 molecule (n) is one of the key parameters for the ORR, which can provide information on both oxygen conversion efficiency and the mechanisms, thus helping to evaluate the performance of electrocatalysts. The rotating ring-disk electrode (RRDE) method[214] and the Koutecky-Levich (KL) method[215] are the two commonest experimental methods to calculate the value of n. The n of PdPt (0.5 M H_2SO_4,[161] 0.1 M $HClO_4$[216]), PdCo (0.1 M $HClO_4$),[217] PdRu (0.1 M KOH),[89] PdAu (0.1 M KOH)[218] alloys, *etc*. were investigated by the RRDE method. Based on the K-L equation, the n values of Pd nanoparticles (both 0.05 M H_2SO_4 and 0.1 M KOH),[219] PdPt (0.1 M KOH,[220] 0.5 M H_2SO_4[221]), PdPb (0.1 M KOH),[154] PdAg (0.1 M KOH)[222]

and PdRh (0.1 M KOH)[223] alloys were reported. Furthermore, some studies verified the n values in both ways, including PdCo (0.5 M H_2SO_4,[135, 224] 0.1 M $HClO_4$[225]), PdNi (0.1 M KOH,[226] both 0.1 M $HClO_4$ and 0.1 M KOH[227]) and PdZn (0.1 M KOH)[88] alloys. These studies showed that the n values are near to four, indicating excellent performance with limited amounts of H_2O_2 generated in the ORR process for these Pd-based electrocatalysts.

However, according to recent studies, n values obtained by the RRDE (n_{RRDE}) and KL (n_{KL}) methods have discrepancies,[42, 224, 228, 229] and n values from the RRDE method are believed to be more accurate. The KL plots are often not linear, and n_{KL} values sometimes exceed theoretical limits. Masa *et al*. proved that the KL plots are affected by the coverage of electrocatalysts on the working electrode and demonstrated that the surface area ratio (total electroactive surface areas to geometric areas of the rotating disc electrode (RDE) surface) should be taken into account when inferring electrocatalytic effects on the basis of KL analysis of RDE data.[230] Zhou *et al*. pointed out that from a theoretical viewpoint, ORR is neither a single-step nor a one-way reaction, therefore does not fulfil the assumptions from the KL method.[231] From an experimental viewpoint, n values are significantly dependent on the angular velocity (ω) of the RDE, contradicting the assumption of constant n in the KL theory. The issues with the RRDE method were also presented in detail by Zhou *et al*.'s study.[231] For example, the collection efficiency (N_C) of the RRDE decreases significantly with the catalyst loading. Moreover, when the electrode surface is rough, N_C also decreases dramatically with ω. In addition, the widely applied RRDE method with a Pt ring is not suitable for H_2O_2 collection in alkaline electrolytes because the oxidation of H_2O_2 on Pt is not the mass-transfer-limited process. A properly biased Au ring rather than Pt ring is more suitable. As a result, the RRDE method with a properly biased Au ring is recommended to determine n values for the ORR in alkaline electrolytes, supplemented by the calibration of the collection efficiency. Therefore, as for Pd-based electrocatalysts, the best possible way is that the RRDE with the relevant calibration is the major approach, and the KL method is an auxiliary verification.

7.2 Electrochemically active surface area (ECSA)

The ECSA of ORR electrocatalysts is a key parameter to evaluate mass activities and specific activities. It can be determined by CO-stripping (oxidation of pre-adsorbed CO monolayers) and

the H_{upd} method (integrated the underpotentially deposited hydrogen (H_{upd}) regions from cyclic voltammetry).[232] In previous work, the ECSAs of PdZn[88] PdAu[157] alloys were estimated by CO-stripping measurements and the ECSAs of PdFe,[155] PdPt[161] alloys were calculated by H_{upd} method, respectively.

It is noted that unlike Pt, Pd could absorb a certain amount of H_2, resulting in the fact that it is impossible to quantitatively differentiate between H_{upd} and absorbed hydrogen (H_{abs}). Therefore, it is hard to obtain the exact ECSA by the H_{upd} method. Recent studies reported that the ECSA of the Pd-based catalyst is measured by the Pd oxide reduction analysis.[233, 234] The Coulomb charge of the Pd-based catalysts is calculated by using the chemically adsorbed oxygen reduction peak instead of the hydrogen adsorption/desorption peak in the Pt-based catalysts. The ECSAs of PdCo,[224, 235] PdPb,[154] PdAg[233] alloys have also been measured by this approach. In addition, the use of underpotentially deposited copper (Cu_{UPD}) is feasible,[236] however, the major disadvantage of this method is that the metal ions might largely affect catalytic reactions. The ECSAs of PdFe alloys[12] were determined by this method.

Shao *et al.* studied the ECSA measurements of Pt- and Pd-based nanoparticles in detail and demonstrated that the ECSAs follow $H_{UPD} <$ CO striping $< Cu_{UPD}$ and Cu_{UPD} is the most accurate method.[237] In Luo *et al.*'s work, the ECSAs of PdMo catalysts were determined by H_{upd}, CO stripping, Cu_{upd} and Pd oxide reduction, and the ECSAs determined from the Cu_{upd} method were used for further analysis.[75]

Some research pointed out that one of the most suitable techniques to determine ECSAs is differential electrochemical mass spectrometry (DEMS),[238] which allows *in-situ* measurements of supported catalysts under controlled mass flow conditions, but this technique is not available in most labs.

7.3 Durability test

Durability is regarded as a key factor for ORR electrocatalysts in practical applications. Durability tests in different studies of Pd-based electrocatalysts varied greatly, and even a small proportion

of studies did not provide specific durability performances. Standard durability test protocols are summarized.

7.3.1 Start/stop cycle and load cycle

The Fuel Cell Commercialization Conference of Japan (FCCJ) proposed several methodologies for evaluating the durability of the membrane electrode assembly (MEA) such as catalysts and membranes in 2007.[239] Proposed potential cycle tests consist of two protocols, the start/stop durability test and the load cycle durability test were revised in 2011.[240] Table 3 shows durability test conditions, protocols, and diagnostic tests for electrocatalysts using half-cell (RDE) and MEA, respectively. Many studies were reported using load cycle protocol to evaluate the durability of electrocatalysts.[241-243]

7.3.2 Accelerated stress test (AST)

The US Department of Energy (DOE) proposed an accelerated stress test protocol in 2007 with the aim of determining the durability and performance of current fuel cell components without the need to test over many years.[205] The associated DOE accelerated stress test protocols and performance metrics are presented in Table 4.

Table 3. Potential-cycle durability test conditions, protocols, and diagnostic test for ORR electrocatalyst. Reproduced with permission.[240] Copyright 2011, IOP Publishing.

Item	Test conditions and protocols		Diagnostic test / Criteria
	Half cell (RDE)	MEA	
Start/stop cycle	1.0 – 1.5 V *vs*. RHE, Triangular-wave potential cycle		· Cyclic voltammetry for ECSA measurement, and ORR activity measurement at every 10 to 1k-cycle. · If ECSA is less than 50 % *vs*. initial values, finish the cycle test. Otherwise, continue up to 60k-cycle.
	25 °C, 0.1 M HClO$_4$, N$_2$ saturated	80 °C, 100 % relative humidity, H$_2$ / N$_2$	
Load cycle	0.6 – 1.0 V *vs.* RHE, Rectangular-wave potential cycle		· Cyclic voltammetry for ECSA measurement, and ORR activity measurement at every 10 to 1k-cycle. · If ECSA is less than 50 % *vs*. initial values, finish the cycle test. Otherwise, continue up to 400k-cycle.
	25 °C, 0.1 M HClO$_4$, N$_2$ saturated	80 °C, 100 % relative humidity, H$_2$ / N$_2$	
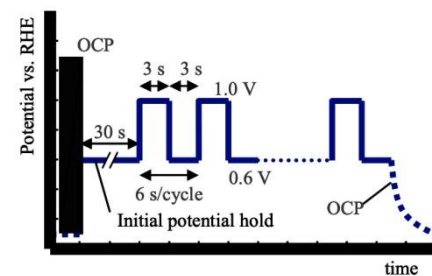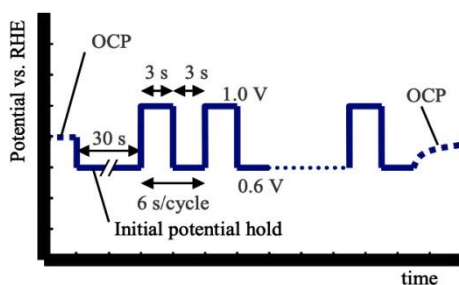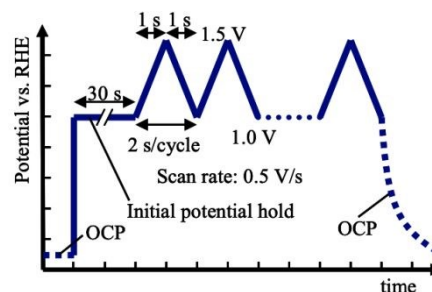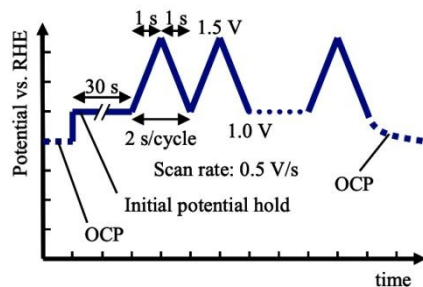
Table 4. DOE AST protocols and metrics for electrocatalysts. Reproduced with permission.[205] Copyright 2007, IOP Publishing.

Cycle	Step change: 30 s at 0.7 V and 30 s at 0.9 V. Single cell 25–50 cm^2
Cycle number	30k
Cycle time	60 s
Temperature	80 °C
Relative humidity	Anode / cathode 100/100%
Fuel/oxidant	H_2 / N_2
Pressure	150 KPa

Metrics	Frequency	Target
Catalytic activity	Start and end of life	≤ 60% loss of initial activity
Polarization curve from 0 to ≥ 1.5 A cm^{-2}	After 0, 1k, 5k, 10k, and 30k cycles	≤ 30 mV loss at 0.8 A cm^{-2}
ECSA/cyclic voltammetry	After 1, 10, 30, 100, 300, 1k, 3k cycles and thereafter every 5k cycles	≤ 40% loss of initial area

7.4 Standardization of electrochemical analysis

Cyclic voltammogram (CV) and linear sweep voltammogram (LSV) on the RDE are extensively collected to evaluate the ORR performance of Pd-based catalysts. These methods allow studying the material in a large potential and time-scale domain, presenting information on the thermodynamic and kinetic behaviors of the electrocatalysts. However, due to the differences in test methods and conditions, it is hard to compare ORR performances of electrocatalysts by MA or SA values. To better compare ORR activities of different electrocatalysts, more standardized and reasonable guidance are needed to be proposed.

Mayrhofer *et al*. scrutinized the thin-film rotating disc electrode (TF-RDE) method for investigating activities of high surface area electrocatalysts.[244] They pointed out: (a) Normalized activities have to be determined. The normalization can be based on the noble metal loading (mass activity) or surface area (specific activity). (b) The active surface area has to be evaluated by

applying a proper method that also considers the capacity of the support. (c) The electrode thickness, the diffusion limited current of the ORR and the current under the specific potential need to be limited.

Garsany *et al*. studied the impact of film drying procedures on RDE characterization and found that films prepared with the rotational drying method are more reproducible than the films prepared with the stationary method.[245] Takahashi *et al*. emphasized the importance of ink preparation for the RDE method.[246]

In different acidic electrolytes, the ORR activity varies. The catalytic activity of Pt/C followed the trend $HClO_4$ > H_2SO_4 > H_3PO_4 and the durability of Pt/C in H_2SO_4 was found to be lower than in $HClO_4$.[246] Pd is less studied in this aspect, but it can be predicted that Pd may exhibit similar trends as Pt. Therefore, it is necessary to unify the types and concentrations of the electrolyte during the test.

Moreover, the ultimate estimation of electrocatalyst catalytic activity towards the ORR should be measured in MEAs. To a certain extent, it can be seen whether the catalyst is suitable for practical applications rather than the laboratory level. For example, Luo *et al*. evaluated the performances of PdMo bimetallene catalysts in Zn-air and Li-air batteries.[75] Hence, the MEAs test is strongly recommended for Pd-based electrocatalysts in future work.

7.5 Summary of electrocatalytic performance of representative Pd-based catalysts
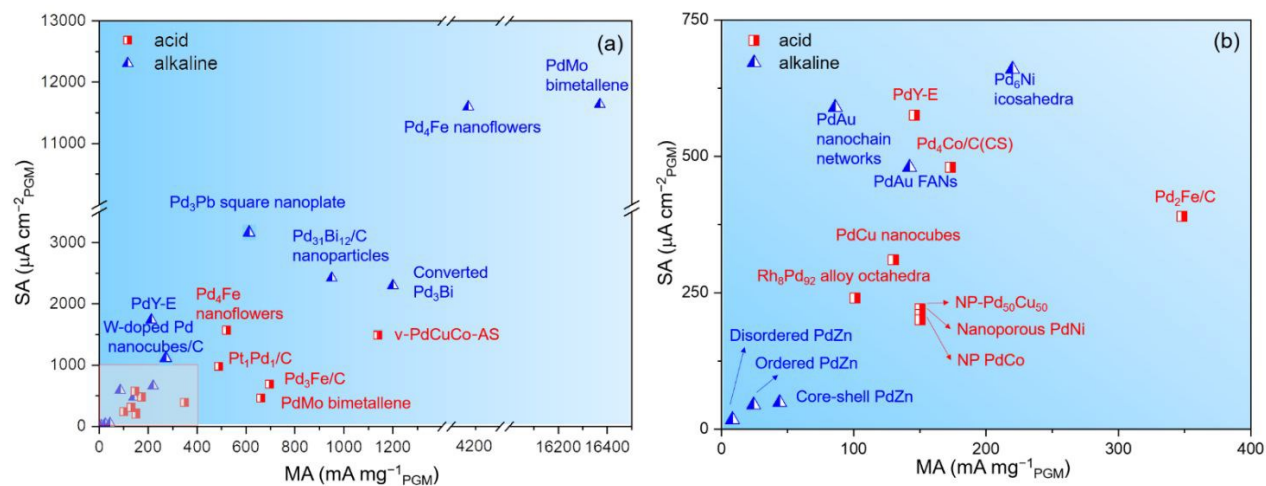
Figure 12. (a) MAs and SAs for different Pd-based catalysts in alkaline and acid media in recent years. (b) Partial enlarged view of (a).

Materials	Mass activity (mA mg^{-1}$_{PGM}$)	Specific activity (µA cm^{-2}$_{PGM}$)	ECSA (m^2 g^{-1})	$E_{1/2}$ (V vs. RHE)	Onset potential (V vs. RHE)	Measured potential (V vs. RHE)	Stability
Disordered PdZn[88]	8.37	17.36	48.2	0.74	0.93	0.85	After continuous operation of about 8 h, the current dropped to 78.30% of its initial value at 0.5 V and 900 rpm.
Ordered PdZn[88]	24.44	44.41	55.04	0.81	0.97	0.85	After continuous operation of about 8 h, the current dropped to 91.58% of its initial value at 0.5 V and 900 rpm.
Core-shell PdZn[88]	44.05	48.83	90.22	0.82	0.98	0.85	After continuous operation of about 8 h, the current dropped to 94.30% of its initial value at 0.5 V and 900 rpm.
Pd$_4$Fe nanoflowers[155]	4070	11600	33	0.903	N/A	0.85	After 5k cycles, the loss of ECSA and MA was 19% and 17%, respectively by cycling the potential between 0.6 and 1.0 V.
Pd$_6$Ni icosahedra[150]	220	660	N/A	0.89	1.04	0.90	After 10k cycles, the catalyst exhibited a 5.6% loss of its initial mass activity by cycling the potential between 0.4 and 1.0 V at 100 mV s^{-1}.
PdAu nanochain networks[157]	86.01	590	45.24	0.848	0.986	0.85	After 1k cycles, the half-wave potentials only negatively shift about 5 mV by sweeping between 0.2 and 1.1 V at 5 mV s^{-1}.
Pd$_{31}$Bi$_{12}$/C nanoparticles[172]	950	2420	N/A	0.92	0.97	0.90	After 10k cycles, retention of ∼60% of the initial activity by cycling the voltage repeatedly between 0.6 and 1.0 V at a sweep rate of 100 mV/s.

Catalyst	MA	SA	ECSA	$E_{1/2}$	E_{onset}	V	Stability
Converted Pd$_3$Bi[180]	1200	2300	N/A	N/A	0.97	0.90	After 10k cycles, the catalyst retained 86% and 69% of the initial SA and MA, respectively, whereas the ECSA decreased by 20%, by cycling the samples from 0.6 to 1.0 V at a sweep rate of 100 mV s^{-1}.
PdY-E[85]	213^a	1740	24	N/A	N/A	0.90	N/A
PdAu FANs[104]	142.21	480	34.5	N/A	N/A	0.90	After 1k cycles, negative shifts of about 7 mV in the half-wave potentials of AuPd FANs, by applying continuous potential sweeps between 0.21 and 1.21 V at a scan rate of 5 mV s^{-1}.
PdMo bimetallene/C[75]	16370	11640	139.7	0.95	N/A	0.90	After 30k cycles, the catalyst retained over 60% of the initial mass activity, by cycling the potential between 0.6 and 1.0 V at 50 mV s^{-1}.
W-doped Pd nanocubes /C[193]	250	1180	21.1	N/A	N/A	0.90	After 10k cycles, the catalyst showed a decrease of 14.8% with respect to the initial mass activity.
Pd$_3$Pb square nanoplate[154]	620	3590	17.3	N/A	N/A	0.90	After 10k cycles, the catalyst showed a 21% loss of its initial mass activity.

Table 5. Summary of electrocatalytic performance of Pd-based catalysts measured by RDE measured in an O$_2$-saturated 0.1 M KOH solution at 1600 rpm at the room temperature, including mass activity (MA), specific activity (SA), electrochemically active surface area (ECSA), half-wave potential ($E_{1/2}$), onset potential (E_{onset}) and measured potential (V). In the stability test, the potential (V) was normalized *vs*. RHE.

^{a} 0.5 M KOH.

Materials	Mass activity (mA mg$^{-1}_{PGM}$)	Specific activity (µA cm$^{-2}_{PGM}$)	ECSA (m^2 g^{-1})	$E_{1/2}$ (V *vs.* RHE)	Measured potential (V *vs.* RHE)	Stability
Pd$_3$Fe/C[12]	696	690	100	0.832	0.80	N/A
Pd$_2$Fe/C[12]	348	390	90	N/A	0.80	N/A
Pd$_4$Co/C(CS)[145]	173	480	~35	N/A	0.75	N/A
Pd$_4$Fe nanoflowers[155]	521	1570	33	0.833	0.85	N/A
Pt$_1$Pd$_1$/C[161]	488 [a]	976	107.7	N/A	0.85	After 10k cycles, the catalyst showed a mass activity loss of only 3.5% by applying linear potential sweeps between 0.5 and 1.0 V at 50 mV s^{-1}.
NP-Pd$_{50}$Cu$_{50}$[82]	150	220	N/A	N/A	0.90	A retention of ~30% of the initial specific activity by using the chronoamperometry method for 3000s at 0.9 V.
Nanoporous PdNi[173]	150	210	N/A	N/A	0.90	After 5k cycles, the catalyst underwent a loss of 12% relative to the initial ECSA with a negative half-wave potential shift by 14 mV from 0.6 to 1.0 V.
Rh$_8$Pd$_{92}$ alloy octahedra[79]	101	240	42.7	N/A	0.90	After 30k cycles, the catalyst showed ~75% of the initial activity between 0.6 and 1.0 V.
NP PdCo[247]	150	200	N/A	N/A	0.90	After 5k cycles, the catalyst showed the degradation with a negative half-wave shift of 19 mV that corresponded to an ~17 % loss of the ECSA between 0.6 and 1.0 V
PdCu nanocubes[152]	130 [b]	310	41.8	0.812	0.85 [c]	N/A
PdY−E[85]	146 [b]	575	24.83	0.851	0.90	N/A

PdMo bimetallene/C[75]	660	~460	139.7	N/A	0.90	Its stability is not sufficient for practical applications.
v-PdCuCo-AS[148]	1135	1610	N/A	N/A	0.80	After 4k cycles between 0.6 and 1.1 V, the catalyst showed a 0.26% loss of MA at 0.9 V.

Table 6. Summary of electrocatalytic performance of Pd-based catalysts measured by RDE at 1600 rpm, 10 mV s^{-1} in a 0.1 M HClO$_4$ solution at room temperature.

[a] 0.5 M H$_2$SO$_4$. [b] 0.1 M H$_2$SO$_4$. [c] V *vs*. NHE

As Tables 5, 6 and Figure 12 show, regarding ORR activity, Pd-based alloy materials had better performance in alkaline electrolytes than in acidic electrolytes, and some of them, such as PdMo bimetallene and Pd_4Fe nanoflowers materials, even exceeded that of Pt-based catalysts. They exhibited excellent ORR activity in alkaline solutions and also had good activity in acidic solutions. However, in acid solution, the stability of Pd alloys catalysts was often not as good as that of Pt-based materials. Indeed, Pd is more susceptible to oxidation at more negative potentials than Pt and is more easily poisoned by anions such as ClO_4^- and other oxygen-containing species as compared to Pt.[10] Pd-based catalysts with different element compositions and morphologies and structures had obvious activity differences. Although previous works have studied the relationship between morphology and activity, there is still no exact direct relationship between material composition, structure and performance. The methods to obtain the expected structure and electrocatalytic performance through experimental preparation is still a challenge.

Other factors, including electrochemically active surface area (ECSA), half wave potential ($E_{1/2}$), Tafel slope, onset potential (E_{onset}), *etc.*, are also the reasons that affect the performance of the electrocatalysts and could not be ignored. Many catalysts reach high mass activities (MAs) by increasing the specific activity (SA) at the extent of a reduced ECSA. In the potential region of kinetic control, low ECSA is counterbalanced by high specific activities. However, at higher overpotentials (usually used in actual systems), the reaction rate that low ECSA causing is not limited by kinetics, but by mass transfer.[248] Therefore, it is necessary to obtain the materials which combine a high mass activity with a high ECSA. In addition, the $E_{1/2}$ is another common parameter that allows comparing the ORR activity of catalysts, especially between platinum group metal (PGM) catalysts and PGM-free catalysts. A positive shift in $E_{1/2}$ indicates a high ORR activity.[249] However, there is an issue that $E_{1/2}$ increases with RDE catalyst loading. Thus, comparisons between catalysts by $E_{1/2}$ are biased towards studies that used higher loading, and loading dependence complicates the comparison between studies of different loadings.[250] Tafel slope, which is derived from the microkinetic model, and thus, represents the reaction mechanism and surface kinetics.[251] Different electrocatalysts show distinct rate-determining steps, such as the dissociation of O_2 or desorption of OH.[251] In general, the smaller the Tafel slope, the faster the ORR kinetics. In the case of cathode Pd-based catalysts, the decrease in onset potential and the

increase in current density detected during the ORR process are considered to be key parameters for evaluating catalyst performance.[252] How to achieve it is the goal that researchers are striving for.

8. Conclusion and perspective
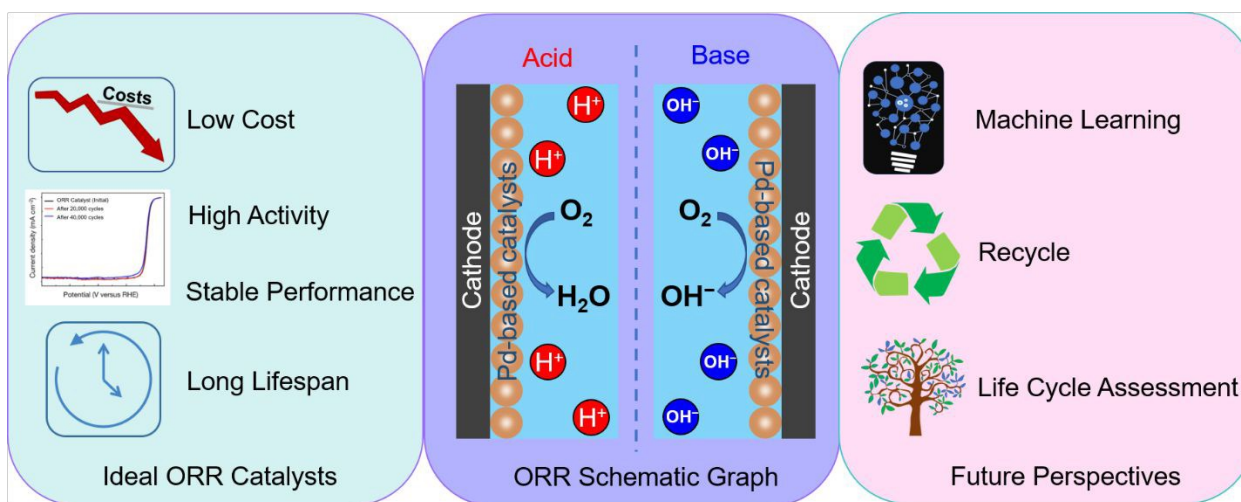
Figure 13. Schematic illustration for the ideal properties and future perspectives on Pd-based alloy electrocatalysts for ORR.

Recent studies on Pd-based alloy catalysts for the oxygen reduction reaction are summarized in this review. There is a trend of rapid development and electrocatalysts are being developed that show excellent activities for the ORR, which often even exceed the performance of Pt-based catalysts, especially in alkaline media and in the presence of methanol. We note that theoretical research often only focuses on one or a few factors, while actual experiments are very complicated. Therefore, the development of related theories and the combination theory with experiments can help us to predict development trends and prepare high-performance materials more efficiently. The alloys formed by palladium and various elements may have good catalytic activity. In addition, Pd alloys with different morphologies and structures can be obtained by different synthesis methods, and their catalytic performance is quite different. Regarding mass activity and specific activity towards ORR, PdMo bimetallene, PdBi alloys and Pd_4Fe nanoflowers materials seem to be the most promising cathode electrocatalysts; however, other parameters, like stability, catalyst activity under actual industrial conditions rather than laboratory conditions, are more important

factors in determining whether commercialization can be achieved. In addition, some other issues for mass production need more attention.

(1) In terms of reaction thermodynamics and kinetics, a more in-depth research is needed to pave the way for future industrialization. The establishment of universal reaction kinetics and thermodynamic models could be achieved through more advanced machine learning techniques for building up correlations to produce high-performance Pd alloys catalysts.

(2) Regarding catalyst deactivation, studies need to focus on deactivation mechanisms, especially for precious metal catalysts. The study of the deactivation mechanism can better understand the catalytic process, thereby helping to extend the service life and understand how to regenerate the catalyst.

(3) As for recycling, it needs to be determined if there is a facile way to regenerate deactivated catalysts. If so, how can this be achieved with efficient circulation and still maintaining high activity and stability. If not, whether the abandoned catalysts can be processed for other applications needs to be studied.

(4) At present, little research has been reported on the life cycle assessment(LCA) of ORR catalysts (not just the Pd or Pt series), so it is difficult to evaluate the environmental impact of these electrocatalysts during the production process. For example, the production of a certain catalyst using low-cost raw materials under harsher reaction conditions is a dilemma. Through LCA, the advantages and disadvantages can be obtained, thus deciding whether this catalyst is worth producing.

In short, the research on Pd-based electrocatalysts towards ORR is moving in the direction of low cost, high activity, stable performance and long lifespan. Researchers need to analyze and solve the above problems to promote the industrialization of this material set, as demonstrated in Figure 13.

Energy & Environmental Science Accepted Manuscript

Appendix A. Supplementary data

1. methodology

1.1.   Data collection

The data was obtained from the Web of Science Core Collection (WoSCC) using the advanced search "TS=("Palladium alloy*" or "Pd* alloy*" or "Palladium catalysts" or "Pd* catalysts") AND TS= ("oxygen reduction reaction" or "ORR")". English was the only chosen language, and the type of documents was restricted to the article. The timespan was from 1970 to 2020. For citation indexes, the data was only selected from Science Citation Index Expanded (SCI-EXPANDED) -- 1970-present. As a result, 400 documents were identified on 6 July 2020.

1.2.   Scientometric analysis methods

1.2.1 Biblioshiny

Biblioshiny, which provides the analysis, presentation and manipulation of data, is a user-friendly interface for bibliometrix.[26] The collected data was extracted in plain text format from WoS. Then RStudio version 1.3.959 was used to export the interface of the biblioshiny by biblometrix under R version 4.0.1. And the data was uploaded to the biblioshiny package. In this work, the extracted data was analysed from annual production, top 10 sources and top 10 countries by production *via* biblioshiny.

1.2.2 CiteSpace

CiteSpace is a free software based on Java environment developed by C. Chen for detecting and visualizing trends and patterns in literature.[27] The data were analysed through CiteSpace version 5.6.5R to visualize the network. This work concentrated on the period from 1997 to 2020 and used 1-year slices.

1.2.3 VOSviewer

VOSviewer is a freely available computer program for constructing and viewing bibliometric maps, which is especially focused on displaying large bibliometric maps in an easy-to-interpret way.[29] The data was analysed *via* VOSviewer version 1.6.15 to obtain the network visualization and density visualization map based on co-keyword.

1.3 Other scientometric analysis on Pd-based alloys for ORR
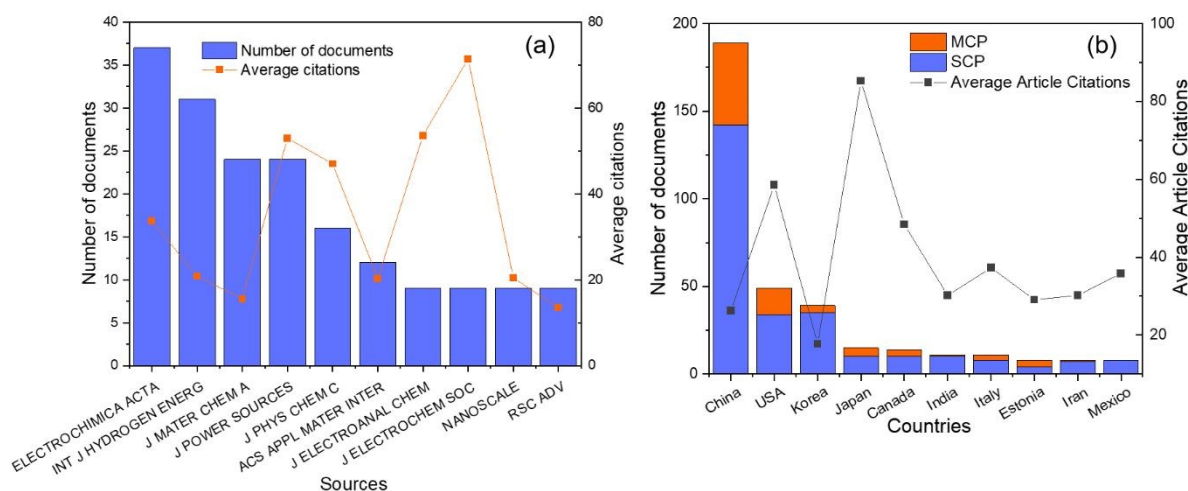
Figure 1*. (a) Top 10 impactful sources and (b) top 10 countries by publications and their average citations on Pd alloys for the oxygen reduction reaction.

Figure 1* (a) described the top 10 sources of these 400 articles. Amongst, *Electrochimica Acta* was the most productive source with 37 articles, which is intended for the studies in the field of electrochemistry. In terms of average citations, *Journal of the Electrochemical Society* (J ELECTROCHEM SOC) was the highest journal, because three highly cited articles (Lee K, 2006[35]; Jiang L, 2009[253]; Wang X, 2008[126]) were published in this journal. Besides, *Journal of Electroanalytical Chemistry* (J ELECTROANAL CHEM), *Journal of Power Sources* (J POWER SOURCES) and *Journal of Physical Chemistry C* (J PHYS CHEM C) had higher average citations.

Figure 1* (b) depicted the top 10 countries by publication numbers. According to all author's addresses, the publications were divided into Single Country Publication (SCP) and Multiple

Country Publication (MCP). China published the most articles (189), which was almost four times that of the USA (ranking the second place). But the average citation was less than that from the USA. Although the number of publications is not high, Japan had the largest average citations. The number of MCP articles to the total number of articles (so-called MCP ratio) could reflect the extent of inter-country collaborations to a certain degree. Estonia and Japan had higher MCP ratios, while Mexico and India had lower ones.

Table 1* displayed the top 10 references with the strongest citation bursts sorted by strength. The centrality value indicates the importance of the position in the network. High values of centrality identify potentially revolutionary publications.[256] Sigma is a hybrid metric, used to measure structural centrality and citation burstness of a cited reference, suggesting the scientific novelty of a document.[257] From Table 1*, 8 in 10 are from cluster #0 (Pd nano-particle).

Among these articles, a paper published by Savadogo[33] in 2004 had the strongest burst strength (17.22), largest sigma value (1.43), longest burst duration (ranging from 2004 to 2012) and longest citation duration (2004−2020). In this work, extremely active palladium-based alloys catalysts without platinum for ORR in an acid solution were shown for the first time. It opened the curtain for the follow-up study of Pd alloy catalysts. In addition, in Gasteiger's article,[255] authors quantified the activities and voltage loss modes for MEAs (membrane electrode assemblies), and provided benchmark oxygen reduction activities for electrocatalysts by using two different testing procedures to establish the relative merit of candidate catalysts. Its centrality was the largest (0.04) and the sigma value was the second largest (1.40). Besides, it is noted that Shao MH was the first author of three references in Table 1*, suggesting that he/she has made outstanding contributions in this field.

Table 1[*] Top 10 references with strongest citation bursts

References	Strength	Centrality	Sigma	Cluster	Duration1997-2020
Savadogo O, 2004, *ELECTROCHEM COMMUN*, V6, P105 [33]	17.22	0.02	1.43	#0	
Shao MH, 2006, *J AM CHEM SOC, V128*, P3526 [36]	13.59	0.02	1.35	#0	
Lee K, 2006, *J ELECTROCHEM SOC*, V153, P0 [186]	13.39	0.01	1.20	#0	
Fernandez JL, 2005, *J AM CHEM SOC*, V127, P357 [91]	13.09	0.02	1.22	#0	
Shao MH, 2006, *LANGMUIR*, V22, P10409 [65]	12.64	0.03	1.40	#0	
Fernandez JL, 2005, *J AM CHEM SOC*, V127, P13100 [83]	11.78	0.01	1.15	#0	
Shao MH, 2016, *CHEM REV*, V116, P3594 [254]	10.58	0.02	1.20	#1	
Gasteiger HA, 2005, *APPL CATAL B-ENVIRON*, V56, P9 [255]	9.19	0.04	1.40	#8	
Raghuveer V, 2005, *J PHYS CHEM B*, V109, P22909 [34]	8.97	0.01	1.12	#0	
Wang WM, 2007*, J POWER SOURCES*, V167, P243 [217]	7.98	0.02	1.17	#0	

Acknowledgement

References

1. J.-P. Randin, *Electrochim. Acta*, 1974, **19**, 83-85.

2. R. Zurilla, R. Sen and E. Yeager, *J. Electrochem. Soc.*, 1978, **125**, 1103-1109.

3. L. Kreja and R. Dabrowski, *J. Power Sources*, 1981, **6**, 35-46.

4. G. Gruver, L. Bregoli, R. Pascoe and H. Kunz, *J. Electrochem. Soc.*, 1978, **125**, 366-366.

5. S. Mukerjee, S. Srinivasan and A. J. Appleby, *Electrochim. Acta*, 1993, **38**, 1661-1669.

6. S. Mukerjee and S. Srinivasan, *J. Electroanal. Chem.*, 1993, **357**, 201-224.

7. K. Kinoshita, *Electrochemical oxygen technology*, John Wiley & Sons, 1992, **30**.

8. Q. Li, T. Wang, D. Havas, H. Zhang, P. Xu, J. Han, J. Cho and G. Wu, *Adv. Sci.*, 2016, **3**, 1600140.

9. M. Rao, A. Damjanovic and J. O. M. Bockris, *J. Phys. Chem.*, 1963, **67**, 2508-2509.

10. M. Shao, *J. Power Sources*, 2011, **196**, 2433-2444.

11. S. T. Nguyen, D. S. L. Tan, J.-M. Lee, S. H. Chan, J. Y. Wang and X. Wang, *Int. J. Hydrogen Energy*, 2011, **36**, 9645-9652.

12. M. Neergat, V. Gunasekar and R. Rahul, *J. Electroanal. Chem.*, 2011, **658**, 25-32.

13. H. Yang, N. Alonso-Vante, C. Lamy and D. L. Akins, *J. Electrochem. Soc.*, 2005, **152**, A704.

14. F. Kadirgan, B. Beden, J. Leger and C. Lamy, *J. Electroanal. Chem. Interfacial Electrochem.*, 1981, **125**, 89-103.

15. R. Moss, H. Gibbens and D. Thomas, *J. Catal.*, 1970, **16**, 117-125.

16. A. Baiker, D. Gasser and J. Lenzner, *J. Chem. Soc., Chem. Commun.*, 1987, 1750-1751.

17.   B. Beden, C. Lamy and J. Leger, *Electrochim. Acta*, 1979, **24**, 1157-1166.

18.   A. Bryant, W. Bugden and J. Pratt, *Acta Metall.*, 1970, **18**, 101-107.

19.   P. Chinh, S. Skalski and J. Budnick, *J. Appl. Phys.*, 1970, **41**, 1080-1080.

20.   G. L. Holleck, *J. Phys. Chem.*, 1970, **74**, 503-511.

21.   T. Skoskiewicz, A. Szafranski and B. Baranowski, *Phys. Status Solidi B*, 1973, **59**, 135-136.

22.   J. Hedman, M. Klasson, R. Nilsson, C. Nordling, M. Sorokina, O. Kljushnikov, S. Nemnonov, V. Trapeznikov and V. Zyryanov, *Phys. Scr.*, 1971, **4**, 195.

23.   E. Allison and G. Bond, *Catal. Rev.*, 1972, **7**, 233-289.

24.   A. Damjanovic and V. Brusić, *Electrochim. Acta*, 1967, **12**, 1171-1184.

25.   R. Pattabiraman, *Appl. Catal., A*, 1997, **153**, 9-20.

26.   M. Aria and C. Cuccurullo, *J. informetr.*, 2017, **11**, 959-975.

27.   M. B. Synnestvedt, C. Chen and J. H. Holmes, *AMIA Annu. Symp. Proc.,* 2005, 724-728.

28.   C. Chen, *Technology J. Am. Soc. Inf. Sci. Technol.*, 2006, **57**, 359-377.

29.   N. J. Van Eck and L. Waltman, *scientometrics*, 2010, **84**, 523-538.

30.   A. Damjanovic and V. Brusić, *J. Electroanal. Chem. Interfacial Electrochem.*, 1967, **15**, 29-33.

31.   J. Fishman and M. Yarish, *Electrochim. Acta*, 1967, **12**, 579-581.

32.   J. Podestá and R. Piatti, *Int. J. Hydrogen Energy*, 1997, **22**, 753-758.

33.   O. Savadogo, K. Lee, K. Oishi, S. Mitsushima, N. Kamiya and K.-I. Ota, *Electrochem. Commun.*, 2004, **6**, 105-109.

34.   V. Raghuveer, A. Manthiram and A. J. Bard, *J. Phys. Chem. B*, 2005, **109**, 22909-22912.

35.   K. Lee, O. Savadogo, A. Ishihara, S. Mitsushima, N. Kamiya and K.-i. Ota, *J. Electrochem. Soc.*, 2006, **153**, A20-A24.

36.   M.-H. Shao, K. Sasaki and R. R. Adzic, *J. Am. Chem. Soc.*, 2006, **128**, 3526-3527.

37.   M. Tarasevich, A. Sadkowski and E. Yeager, *Compr. Treatise Electrochem.*, Springer, 1983, 301-398.

38.   E. Yeager, *Electrochim. Acta*, 1984, **29**, 1527-1537.

39.   T. Jacob and W. A. Goddard III, *ChemPhysChem*, 2006, **7**, 992-1005.

40.   N. Anastasijević, V. Vesović and R. Adžić, *J. Electroanal. Chem. Interfacial Electrochem.*, 1987, **229**, 317-325.

41.   M.-h. Shao, P. Liu and R. R. Adzic, *J. Am. Chem. Soc.*, 2006, **128**, 7408-7409.

42.   J.-D. Kim, S.-I. Pyun, T.-H. Yang and J.-B. Ju, *J. Electroanal. Chem.*, 1995, **383**, 161-166.

43.   Y. Sha, T. H. Yu, B. V. Merinov, P. Shirvanian and W. A. Goddard III, *J. Phys. Chem. Lett.*, 2011, **2**, 572-576.

44.   D. C. Ford, A. U. Nilekar, Y. Xu and M. Mavrikakis, *Surf. Sci.*, 2010, **604**, 1565-1575.

45.   E. López-Chávez, A. Garcia-Quiroz, G. González-García, Y. A. Peña-Castañeda, J. A. Díaz-Góngora and F. de Landa Castillo-Alvarado, *Int. J. Hydrogen Energy*, 2016, **41**, 23281-23286.

46.   T. T. Vo Doan, J. Wang, K. C. Poon, D. C. Tan, B. Khezri, R. D. Webster, H. Su and H. Sato, *Angew. Chem. Int. Ed.*, 2016, **55**, 6842-6847.

47.   X. Ge, A. Sumboja, D. Wuu, T. An, B. Li, F. T. Goh, T. A. Hor, Y. Zong and Z. Liu, *ACS Catal.*, 2015, **5**, 4643-4667.

48.   R. Rahul, R. Singh, B. Bera, R. Devivaraprasad and M. Neergat, *Phys. Chem. Chem. Phys.*, 2015, **17**, 15146-15155.

49.   Y. H. Wang, J. B. Le, W. Q. Li, J. Wei, P. M. Radjenovic, H. Zhang, X. S. Zhou, J. Cheng, Z. Q. Tian and J. F. Li, *Angew. Chem.*, 2019, **131**, 16208-16212.

50.   Q. Jia, K. Caldwell, J. M. Ziegelbauer, A. Kongkanand, F. T. Wagner, S. Mukerjee and D. E. Ramaker, *J. Electrochem. Soc.*, 2014, **161**, F1323.

51.   S. Sharma, C. Zeng and A. A. Peterson, *J. Chem. Phys.*, 2019, **150**, 041704.

52.   Q. Zhang and A. Asthagiri, *Catal. Today*, 2019, **323**, 35-43.

53.   H.-C. Tsai, Y.-C. Hsieh, T. H. Yu, Y.-J. Lee, Y.-H. Wu, B. V. Merinov, P.-W. Wu, S.-Y. Chen, R. R. Adzic and W. A. Goddard III, *ACS Catal.*, 2015, **5**, 1568-1580.

54.   X. Wang, X. Li, S. Liao and B. Li, *Comput. Mater. Sci.*, 2018, **149**, 107-114.

55.   L. Ou and S. Chen, *J. Phys. Chem. C*, 2013, **117**, 1342-1349.

56.   Y. Sha, T. H. Yu, B. V. Merinov and W. A. Goddard III, *ACS Catal.*, 2014, **4**, 1189-1197.

57.   I. Roche and K. Scott, *J. Appl. Electrochem.*, 2009, **39**, 197-204.

58.   Y.-W. Lee, S.-E. Oh and K.-W. Park, *Electrochem. Commun.*, 2011, **13**, 1300-1303.

59.   F. Harnisch and U. Schröder, *Chem. Soc. Rev.*, 2010, **39**, 4433-4448.

60.   S. Rojas-Carbonell, C. Santoro, A. Serov and P. Atanassov, *Electrochem. Commun.*, 2017, **75**, 38-42.

61.   J. K. Nørskov, J. Rossmeisl, A. Logadottir, L. Lindqvist, J. R. Kitchin, T. Bligaard and H. Jonsson, *J. Phys. Chem. B*, 2004, **108**, 17886-17892.

62.   J. L. Fernández, J. M. White, Y. Sun, W. Tang, G. Henkelman and A. J. Bard, *Langmuir*, 2006, **22**, 10426-10431.

63.   A. Appleby, *Catal. Rev.*, 1971, **4**, 221-244.

64.   V. Stamenkovic, B. S. Mun, K. J. Mayrhofer, P. N. Ross, N. M. Markovic, J. Rossmeisl, J. Greeley and J. K. Nørskov, *Angew. Chem. Int. Ed.*, 2006, **45**, 2897-2901.

65.   M. Shao, T. Huang, P. Liu, J. Zhang, K. Sasaki, M. Vukmirovic and R. Adzic, *Langmuir*, 2006, **22**, 10409-10415.

66.   M. Shao, P. Liu, J. Zhang and R. Adzic, *J. Phys. Chem. B*, 2007, **111**, 6772-6775.

67.   Y. Suo, L. Zhuang and J. Lu, *Angew. Chem. Int. Ed.*, 2007, **46**, 2862-2864.

68.   L. Qi and J. Li, *J. Catal.*, 2012, **295**, 59-69.

69.   B. Hammer and J. K. Norskov, *Nature*, 1995, **376**, 238-240.

70.   B. Hammer, Y. Morikawa and J. K. Nørskov, *Phys. Rev. Lett.*, 1996, **76**, 2141.

71.   A. Ruban, B. Hammer, P. Stoltze, H. L. Skriver and J. K. Nørskov, *J. Mol. Catal. A: Chem.*, 1997, **115**, 421-429.

72.   B. Hammer and J. Nørskov, *Surf. Sci.*, 1995, **343**, 211-220.

73.   L. A. Kibler, A. M. El-Aziz, R. Hoyer and D. M. Kolb, *Angew. Chem. Int. Ed.*, 2005, **44**, 2080-2084.

74.   B. S. Mun, C. Lee, V. Stamenkovic, N. M. Markovic and P. N. Ross Jr, *Phys. Rev. B*, 2005, **71**, 115420.

75.   M. Luo, Z. Zhao, Y. Zhang, Y. Sun, Y. Xing, F. Lv, Y. Yang, X. Zhang, S. Hwang and Y. Qin, *Nature*, 2019, **574**, 81-85.

76.   J. W. Hong, S. W. Kang, B.-S. Choi, D. Kim, S. B. Lee and S. W. Han, *ACS nano*, 2012, **6**, 2410-2419.

77.   H. Duan and C. Xu, *Phys. Chem. Chem. Phys.*, 2016, **18**, 4166-4173.

78.   J. Zhao, A. Sarkar and A. Manthiram, *Electrochim. Acta*, 2010, **55**, 1756-1765.

79.   Y. Yan, F. Zhan, J. Du, Y. Jiang, C. Jin, M. Fu, H. Zhang and D. Yang, *Nanoscale*, 2015, **7**, 301-307.

80.   L. E. Betancourt, A. Rojas-Pérez, I. Orozco, A. I. Frenkel, Y. Li, K. Sasaki, S. D. Senanayake and C. R. Cabrera, *ACS Appl. Energy Mater.*, 2020, **3**, 2342-2349.

81.   J.-J. Lv, S.-S. Li, A.-J. Wang, L.-P. Mei, J.-R. Chen and J.-J. Feng, *Electrochim. Acta*, 2014, **136**, 521-528.

82.   H. Zhang, Q. Hao, H. Geng and C. Xu, *Int. J. Hydrogen Energy*, 2013, **38**, 10029-10038.

83.   J. L. Fernández, V. Raghuveer, A. Manthiram and A. J. Bard, *J. Am. Chem. Soc.*, 2005, **127**, 13100-13101.

84.   S. Salomé, A. Ferraria, A. B. Do Rego, F. Alcaide, O. Savadogo and R. Rego, *Electrochim. Acta*, 2016, **192**, 268-282.

85.   R. Brandiele, V. Amendola, A. Guadagnini, G. A. Rizzi, D. Badocco, P. Pastore, A. A. Isse, C. Durante and A. Gennaro, *Electrochim. Acta*, 2019, **320**, 134563.

86.   X. Lu, M. Ahmadi, F. J. DiSalvo and H. D. Abruña, *ACS Catal.*, 2020, **10**, 5891-5898.

87.   Y. Dai, P. Yu, Q. Huang and K. Sun, *Fuel Cells*, 2016, **16**, 165-169.

88.   H. Yang, K. Wang, Z. Tang, Z. Liu and S. Chen, *J. Catal.*, 2020, **382**, 181-191.

89.   J. Tian, W. Wu, Z. Tang, Y. Wu, R. Burns, B. Tichnell, Z. Liu and S. Chen, *Catalysts*, 2018, **8**, 329.

90.   H. C. Ham, D. Manogaran, K. H. Lee, K. Kwon, S.-a. Jin, D. J. You, C. Pak and G. S. Hwang, *J. Chem. Phys.*, 2013, 201104.

91.   J. L. Fernández, D. A. Walsh and A. J. Bard, *J. Am. Chem. Soc.*, 2005, **127**, 357-365.

92.   Y. Wang and P. B. Balbuena, *J. Phys. Chem. B*, 2005, **109**, 18902-18906.

93.   W. Tang, L. Zhang and G. Henkelman, *J Phys. Chem. Lett.*, 2011, **2**, 1328-1331.

94.   W. Tang and G. Henkelman, *J. Chem. Phys.*, 2009, **130**, 194504.

95.   F. Fouda-Onana, S. Bah and O. Savadogo, *J. Electroanal. Chem.*, 2009, **636**, 1-9.

96.   H. Guo, J. A. Trindell, H. Li, D. Fernandez, S. M. Humphrey, G. Henkelman and R. M. Crooks, *J. Mater. Chem. A*, 2020, **8**, 8421-8429.

97.   J. A. Trindell, Z. Duan, G. Henkelman and R. M. Crooks, *ChemElectroChem*, 2020, **7**, 3824-3831.

98.   L. Ou, *J. Chem.*, 2015, **2015**.

99.   B. Han, C. E. Carlton, J. Suntivich, Z. Xu and Y. Shao-Horn, *J. Phys. Chem. C*, 2015, **119**, 3971-3978.

100. V. Stamenkovic, B. S. Mun, K. J. Mayrhofer, P. N. Ross, N. M. Markovic, J. Rossmeisl, J. Greeley and J. K. Nørskov, *Angew. Chem.*, 2006, **118**, 2963-2967.

101. S. Zuluaga and S. Stolbov, *J. Chem. Phys.*, 2011, **135**, 134702.

102. D. Chen, C. Li, H. Liu, F. Ye and J. Yang, *Sci. Rep.*, 2015, **5**, 11949.

103. Y. Xiong, H. Shan, Z. Zhou, Y. Yan, W. Chen, Y. Yang, Y. Liu, H. Tian, J. Wu and H. Zhang, *Small*, 2017, **13**, 1603423.

104. L.-L. He, P. Song, A.-J. Wang, J.-N. Zheng, L.-P. Mei and J.-J. Feng, *J. Mater. Chem. A*, 2015, **3**, 5352-5359.

105. X. Wang, S.-I. Choi, L. T. Roling, M. Luo, C. Ma, L. Zhang, M. Chi, J. Liu, Z. Xie and J. A. Herron, *Nat. Commun.*, 2015, **6**, 7594.

106. D. Wang, H. L. Xin, H. Wang, Y. Yu, E. Rus, D. A. Muller, F. J. DiSalvo and H. D. Abruña, *Chem. Mater.*, 2012, **24**, 2274-2281.

107. W. Xiao, M. A. L. Cordeiro, M. Gong, L. Han, J. Wang, C. Bian, J. Zhu, H. L. Xin and D. Wang, *J. Mater. Chem. A*, 2017, **5**, 9867-9872.

108. W. Zhou, M. Li, O. L. Ding, S. H. Chan, L. Zhang and Y. Xue, *Int. J. Hydrogen Energy*, 2014, **39**, 6433-6442.

109. L. Jiang, A. Hsu, D. Chu and R. Chen, *J. Electrochem. Soc.*, 2009, **156**, B643-B649.

110. M. V. Castegnaro, W. J. Paschoalino, M. R. Fernandes, B. Balke, M. C. M. Alves, E. A. Ticianelli and J. Morais, *Langmuir*, 2017, **33**, 2734-2743.

111. S. Kondo, M. Nakamura, N. Maki and N. Hoshi, *J. Phys. Chem. C*, 2009, **113**, 12625-12628.

112. A. Hitotsuyanagi, S. Kondo, M. Nakamura and N. Hoshi, *J. Electroanal. Chem.*, 2011, **657**, 123-127.

113. L. Xiao, L. Zhuang, Y. Liu and J. Lu, *J. Am. Chem. Soc.*, 2009, **131**, 602-608.

114. M. Shao, T. Yu, J. H. Odell, M. Jin and Y. Xia, *Chem. Commun.*, 2011, **47**, 6566-6568.

115. H. Erikson, A. Sarapuu, K. Tammeveski, J. Solla-Gullón and J. M. Feliu, *Electrochem. Commun.*, 2011, **13**, 734-737.

116. P. Strasser and S. Kühl, *Nano Energy*, 2016, **29**, 166-177.

117.   P. Strasser, *Handbook of Fuel Cells*, 2010.

118.   S. Tominaka, T. Hayashi, Y. Nakamura and T. Osaka, *J. Mater. Chem.* 2010, **20**, 7175-7182.

119.   T. Gunji, S. H. Noh, F. Ando, T. Tanabe, B. Han, T. Ohsaka and F. Matsumoto, *J. Mater. Chem. A*, 2018, **6**, 14828-14837.

120.   H. Duan and C. Xu, *J. Power Sources*, 2016, **316**, 106-113.

121.   H.-F. Yang, Y.-Y. Feng, L.-X. Du, Z.-H. Liu and D.-S. Kong, *RSC Adv.*, 2016, **6**, 16904-16910.

122.   R. Yang, W. Bian, P. Strasser and M. F. Toney, *J. Power Sources*, 2013, **222**, 169-176.

123.   S. Mondal and C. R. Raj, *ACS Appl. Mater. Interfaces*, 2019, **11**, 14110-14119.

124.   C.-L. Lee, K.-L. Huang, Y.-L. Tsai and Y.-J. Chao, *Electrochem. Commun.*, 2013, **34**, 282-285.

125.   M. Ramanathan, B. Li, J. Greeley and J. Prakash, *ECS Trans.*, 2010, **33**, 181.

126.   X. Wang, N. Kariuki, J. T. Vaughey, J. Goodpaster, R. Kumar and D. J. Myers, *J. Electrochem. Soc.*, 2008, **155**, B602.

127.   J. Yang, W. Zhou, C. H. Cheng, J. Y. Lee and Z. Liu, *ACS Appl. Mater. Interfaces*, 2010, **2**, 119-126.

128.   M. Ramanathan, V. Ramani and J. Prakash, *Electrochim. Acta*, 2012, **75**, 254-261.

129.   T. Gunji, R. H. Wakabayashi, S. H. Noh, B. Han, F. Matsumoto, F. J. DiSalvo and H. D. Abruña, *Electrochim. Acta*, 2018, **283**, 1045-1052.

130.   Y. Zheng, L. Zhang, P. He, D. Dang, Q. Zeng, J. Zeng and M. Liu, *Electrocatalysis*, 2018, **9**, 495-504.

131.   K. Maiti, J. Balamurugan, S. G. Peera, N. H. Kim and J. H. Lee, *ACS Appl. Mater. Interfaces*, 2018, **10**, 18734-18745.

132.   A. M. Remona and K. Phani, *J. Fuel Cell Sci. Technol.*, 2011, **8**.

133.   G. Ramos-Sánchez, M. M. Bruno, Y. R. Thomas, H. R. Corti and O. Solorza-Feria, *Int. J. Hydrogen Energy*, 2012, **37**, 31-40.

134.   Z. Liu, X. Yang, L. Cui, Z. Shi, B. Lu, X. Guo, J. Zhang, L. Xu, Y. Tang and Y. Xiang, *Part. Part. Syst. Charact.*, 2018, **35**, 1700366.

135.   L. Zhang, K. Lee and J. Zhang, *Electrochim. Acta*, 2007, **52**, 3088-3094.

136.   S.-Y. Ang and D. A. Walsh, *Appl. Catal., B,* 2010, **98**, 49-56.

137.   W. Li, Z. Le, T. Zhou, M. Liao, H. Liu, B. Na, Y. Yu, B. Wang, H. Zhou and Z. Liao, *Int. J. Electrochem. Sci*, 2018, **13**, 9292-9301.

138.   G. R. Xu, C. C. Han, Y. Y. Zhu, J. H. Zeng, J. X. Jiang and Y. Chen, *Adv. Mater. Interfaces*, 2018, **5**, 1701322.

139.   Y. Zhao, Y. Ding, B. Qiao, K. Zheng, P. Liu, F. Li, S. Li and Y. Chen, *J. Mater. Chem. A*, 2018, **6**, 17771-17777.

140.   H.-M. Liu, S.-H. Han, Y.-Y. Zhu, P. Chen and Y. Chen, *Green Energy Environ.*, 2018, **3**, 375-383.

141.   S. An, J.-H. Park, C.-H. Shin, J. Joo, E. Ramasamy, J. Hwang and J. Lee, *Carbon*, 2011, **49**, 1108-1117.

142.   N. V. Long, T. D. Hien, T. Asaka, M. Ohtaki and M. Nogami, *Int. J. Hydrogen Energy*, 2011, **36**, 8478-8491.

143.   J. Liu, J. Yin, B. Feng, F. Li and F. Wang, *Appl. Surf. Sci.*, 2019, **473**, 318-325.

144.   A. T. N. Nguyen and J. H. Shim, *J Electroanal. Chem.*, 2018, **827**, 120-127.

145.   J.-H. Jang, C. Pak and Y.-U. Kwon, *J. Power Sources*, 2012, **201**, 179-183.

146.   F. Pires and H. Villullas, *Int. J. Hydrogen Energy*, 2012, **37**, 17052-17059.

147.   L. Bu, N. Zhang, S. Guo, X. Zhang, J. Li, J. Yao, T. Wu, G. Lu, J.-Y. Ma and D. Su, *Science*, 2016, **354**, 1410-1414.

148.   Y. Zuo, D. Rao, S. Li, T. Li, G. Zhu, S. Chen, L. Song, Y. Chai and H. Han, *Adv. Mater.*, 2018, **30**, 1704171.

149.   H. Wang, W. Luo, L. Zhu, Z. Zhao, B. E, W. Tu, X. Ke, M. Sui, C. Chen and Q. Chen, *Adv. Funct. Mater.*, 2018, **28**, 1707219.

150.   Y. Feng, Q. Shao, Y. Ji, X. Cui, Y. Li, X. Zhu and X. Huang, *Sci. Adv.*, 2018, **4**, eaap8817.

151.   L. B. Venarusso, C. V. Boone, J. Bettini and G. Maia, *J. Mater. Chem. A*, 2018, **6**, 1714-1726.

152.   L. Zhang, F. Hou and Y. Tan, *Chem. Commun.*, 2012, **48**, 7152-7154.

153.   X. Jiang, Y. Xiong, Y. Wang, J. Wang, N. Li, J. Zhou, G. Fu, D. Sun and Y. Tang, *J. Mater. Chem. A*, 2019, **7**, 5248-5257.

154. S. Luo, M. Tang, X. Wu, Y. Ou, Z. Wang, N. Jian, X. Li, Y. Lin, Y. Yan and J. Huang, *CrystEngComm*, 2019, **21**, 290-296.

155. C. Lian, Y. Cheng, L. Chen, X. Han, X. Lei, Y. Liu and Y. Wang, *Chem. Commun.*, 2018, **54**, 7058-7061.

156. Z. Cui, H. Chen, M. Zhao and F. J. DiSalvo, *Nano Lett.*, 2016, **16**, 2560-2566.

157. L.-L. He, P. Song, J.-J. Feng, W.-H. Huang, Q.-L. Wang and A.-J. Wang, *Electrochim. Acta*, 2015, **176**, 86-95.

158. L. Kuai, X. Yu, S. Wang, Y. Sang and B. Geng, *Langmuir*, 2012, **28**, 7168-7173.

159. Y. Ma, L. Yin, G. Cao, Q. Huang, M. He, W. Wei, H. Zhao, D. Zhang, M. Wang and T. Yang, *Small*, 2018, **14**, 1703613.

160. X. Peng, Z. Cui, X. Bai and H. Lv, *IET nanobiotechnol.*, 2018, **12**, 1031-1036.

161. W. Wang, Z. Wang, J. Wang, C. J. Zhong and C. J. Liu, *Adv. Sci.*, 2017, **4**, 1600486.

162. M. Yang, Z. Wang, W. Wang and C.-j. Liu, *Nanoscale Res. Lett.*, 2014, **9**, 405.

163. G. Zangari, *Coatings*, 2015, **5**, 195-218.

164. E. Herrero, L. J. Buller and H. D. Abruña, *Chem. Rev.*, 2001, **101**, 1897-1930.

165. S. R. Brankovic and G. Zangari, *Electrochemical Engineering Across Scales: From Molecules to Processes*, 2015.

166. A. Brenner, *Electrodeposition of alloys: principles and practice*, Elsevier, 2013.

167. F. Gobal and R. Arab, *J. Electroanal. Chem.*, 2010, **647**, 66-73.

168. Y. Sun, B. T. Mayers and Y. Xia, *Nano Lett.*, 2002, **2**, 481-485.

169. Y. Sun, B. Mayers and Y. Xia, *Adv. Mater.*, 2003, **15**, 641-646.

170. C. Xu, Y. Zhang, L. Wang, L. Xu, X. Bian, H. Ma and Y. Ding, *Chem. Mater.*, 2009, **21**, 3110-3116.

171. V. Richoux, S. Diliberto, C. Boulanger and J. Lecuire, *Electrochim. Acta*, 2007, **52**, 3053-3060.

172. Y. Wang and A. S. Hall, *ACS Energy Lett.*, 2019, **5**, 17-22.

173. C. Xu, Y. Liu, Q. Hao and H. Duan, *J. Mater. Chem. A*, 2013, **1**, 13542-13548.

174. P. Strasser, S. Koh, T. Anniyev, J. Greeley, K. More, C. Yu, Z. Liu, S. Kaya, D. Nordlund and H. Ogasawara, *Nat. Chem.*, 2010, **2**, 454-460.

175. Y. Liu and C. Xu, *ChemSusChem*, 2013, **6**, 78-84.

176. J. Chen, Y. Li, N. Lu, C. Tian, Z. Han, L. Zhang, Y. Fang, B. Qian, X. Jiang and R. Cui, *J. Mater. Chem. A*, 2018, **6**, 23560-23568.

177. H. Begum, M. S. Ahmed, S. Cho and S. Jeon, *Int. J. Hydrogen Energy*, 2018, **43**, 229-238.

178. L. Sun, C.-L. Chien and P. C. Searson, *Chem. Mater.*, 2004, **16**, 3125-3129.

179. Q. Zhang and Z. Zhang, *Phys. Chem. Chem. Phys.*, 2010, **12**, 1453-1472.

180. D. Sun, Y. Wang, K. J. Livi, C. Wang, R. Luo, Z. Zhang, H. Alghamdi, C. Li, F. An and B. Gaskey, *ACS nano*, 2019, **13**, 10818-10825.

181. T. Tsuji, Y. Higashi, M. Tsuji, Y. Ishikawa and N. Koshizaki, *Appl. Surf. Sci.,* 2015, **348**, 10-15.

182. W.-L. Chan, R. S. Averback, D. G. Cahill and A. Lagoutchev, *Phys. Rev. B*, 2008, **78**, 214107.

183. Y. Han, S. Wu, E. Dai, Y. Ye, J. Liu, Z. Tian, Y. Cai, X. Zhu and C. Liang, *ChemPhysChem*, 2017, **18**, 1133-1139.

184. H. Zheng, M. S. Matseke and T. S. Munonde, *Ultrason. Sonochem.*, 2019, **57**, 166-171.

185. Ş. Korkmaz, B. Gecici, S. D. Korkmaz, R. Mohammadigharehbagh, S. Pat, S. Özen, V. Şenay and H. H. Yudar, *Vacuum*, 2016, **131**, 142-146.

186. K. Lee, O. Savadogo, A. Ishihara, S. Mitsushima, N. Kamiya and K.-i. Ota, *J. Electrochem. Soc.*, 2005, **153**, A20.

187. M. Tarasevich, G. Zhutaeva, V. Bogdanovskaya, M. Radina, M. Ehrenburg and A. Chalykh, *Electrochim. Acta*, 2007, **52**, 5108-5118.

188. N. Pokhrel, P. K. Vabbina and N. Pala, *Ultrason. Sonochem.*, 2016, **29**, 104-128.

189. L. Karuppasamy, S. Anandan, C.-Y. Chen and J. J. Wu, *Electrocatalysis*, 2017, **8**, 430-441.

190. D.-S. Kim, J.-H. Kim, I.-K. Jeong, J. K. Choi and Y.-T. Kim, *J. Catal.*, 2012, **290**, 65-78.

191. Q. Hu, W. Zhan, Y. Guo, L. Luo, R. Zhang, D. Chen and X. Zhou, *J. Energy Chem.*, 2020, **40**, 217-223.

192. Y. Sun, B. Huang, N. Xu, Y. Li, M. Luo, C. Li, Y. Qin, L. Wang and S. Guo, *Sci. Bull.*, 2019, **64**, 54-62.

193. F. Ahmad, L. Luo, X. Li, H. Huang and J. Zeng, *Chin. J. Catal.*, 2018, **39**, 1202-1209.

194. Y.-C. Wei, C.-W. Liu and K.-W. Wang, *Chem. Commun.*, 2011, **47**, 11927-11929.

195. W.-D. Kang, Y.-C. Wei, C.-W. Liu and K.-W. Wang, *Electrochem. Commun.*, 2011, **13**, 162-165.

196. Q. Yang, L. Shi, B. Yu, J. Xu, C. Wei, Y. Wang and H. Chen, *J. Mater. Chem. A*, 2019, **7**, 18846-18851.

197. J.-X. Feng, S.-Y. Tong, Y.-X. Tong and G.-R. Li, *J. Am. Chem. Soc.*, 2018, **140**, 5118-5126.

198. J. C. Calderón, L. Ndzuzo, B. J. Bladergroen and S. Pasupathi, *Int. J. Hydrogen Energy*, 2018, **43**, 16881-16896.

199. M. Thi, T. Tran, P. H. Anh, H.-T. Nhac-Vu and Q. Bui, *J. Alloys Compd.*, 2019, **797**, 314-324.

200. M. Martins, Ö. Metin, B. Šljukić, M. Sevim, C. Sequeira and D. Santos, *Int. J. Hydrogen Energy*, 2019, **44**, 14193-14200.

201. Y. Chen, X. Jiang, Y. Li, P. Li, Q. Liu, G. Fu, L. Xu, D. Sun and Y. Tang, *Adv. Mater. Interfaces*, 2018, **5**, 1701015.

202. J. Ju, X. Wang and W. Chen, *Int. J. Hydrogen Energy*, 2020, **45**, 6437-6446.

203. G. Li, B. Shi, Y. Gong, Y. Zhang, X. Wang, M. Guo and X. Lyu, *Mater. Chem. Phys.*, 2020, **243**, 122570.

204. M. Lüsi, H. Erikson, A. Sarapuu, M. Merisalu, M. Rähn, A. Treshchalov, P. Paiste, M. Käärik, J. Leis and V. Sammelselg, *ChemElectroChem*, 2020, **7**, 546-554.

205. Garland, Nancy, Thomas Benjamin, and John Kopasz, *ECS Trans.*, 2007, **11**, 923.

206. H. Liu, W. Li and A. Manthiram, *Appl. Catal. B: Environ.*, 2009, **90**, 184-194.

207. D. J. You, D. H. Kim, J. R. De Lile, C. Li, S. G. Lee, J. M. Kim and C. Pak, *Appl. Catal. A: Gen.*, 2018, **562**, 250-257.

208. Q. Gong, S. Gong, T. Zhang, X. Cheng and H. Li, *J. Electrochem. Soc.*, 2019, **166**, F906.

209. Y. Zhang, B. Huang, G. Luo, T. Sun, Y. Feng, Y. Wang, Y. Ma, Q. Shao, Y. Li and Z. Zhou, *Sci. Adv.*, 2020, **6**, eaba9731.

210. A. Albarbar and M. Alrweq, *Proton Exchange Membrane Fuel Cells*, 2018, 9-29.

211. M. Pourbaix, *NACE*, 1974, **307**.

212. J. Solla-Gullon, V. Montiel, A. Aldaz and J. Clavilier, *Electrochem. Commun.*, 2002, **4**, 716-721.

213. P. Wells, E. Crabb, C. King, R. Wiltshire, B. Billsborrow, D. Thompsett and A. Russell, *Phys. Chem. Chem. Phys.*, 2009, **11**, 5773-5781.

214. U. Paulus, T. Schmidt, H. Gasteiger and R. Behm, *J. Electroanal. Chem.*, 2001, **495**, 134-145.

215. O. El Mouahid, C. Coutanceau, E. Belgsir, P. Crouigneau, J. Léger and C. Lamy, *J. Electroanal. Chem.*, 1997, **426**, 117-123.

216. W. Wang, Q. Huang, J. Liu, Z. Zou, Z. Li and H. Yang, *Electrochem. Commun.*, 2008, **10**, 1396-1399.

217. W. Wang, D. Zheng, C. Du, Z. Zou, X. Zhang, B. Xia, H. Yang and D. L. Akins, *J. Power Sources*, 2007, **167**, 243-249.

218. W. Yan, Z. Tang, L. Wang, Q. Wang, H. Yang and S. Chen, *Int. J. Hydrogen Energy*, 2017, **42**, 218-227.

219. H. Erikson, A. Sarapuu, N. Alexeyeva, K. Tammeveski, J. Solla-Gullón and J. Feliu, *Electrochim. Acta*, 2012, **59**, 329-335.

220. X. Zhong, Y. Qin, X. Chen, W. Xu, G. Zhuang, X. Li and J. Wang, *Carbon*, 2017, **114**, 740-748.

221. K. Jukk, N. Kongi, K. Tammeveski, J. Solla-Gullón and J. M. Feliu, *Electrochem. Commun.*, 2015, **56**, 11-15.

222. L. Xu, Z. Luo, Z. Fan, X. Zhang, C. Tan, H. Li, H. Zhang and C. Xue, *Nanoscale*, 2014, **6**, 11738-11743.

223. Y. Qi, J. Wu, H. Zhang, Y. Jiang, C. Jin, M. Fu, H. Yang and D. Yang, *Nanoscale*, 2014, **6**, 7012-7018.

224. P. Chandran, A. Ghosh and S. Ramaprabhu, *Sci. Rep.*, 2018, **8**, 1-11.

225. X. Li, Q. Huang, Z. Zou, B. Xia and H. Yang, *Electrochim. Acta*, 2008, **53**, 6662-6667.

226. B. Li and J. Prakash, *Electrochem. Commun.*, 2009, **11**, 1162-1165.

227. J. Jiang, H. Gao, S. Lu, X. Zhang, C.-Y. Wang, W.-K. Wang and H.-Q. Yu, *J. Mater. Chem. A*, 2017, **5**, 9233-9240.

228. Y. Zheng, Y. Jiao, L. Ge, M. Jaroniec and S. Z. Qiao, *Angew. Chem.*, 2013, **125**, 3192-3198.

229.   J. Duan, Y. Zheng, S. Chen, Y. Tang, M. Jaroniec and S. Qiao, *Chem. Commun.*, 2013, **49**, 7705-7707.

230.   J. Masa, C. Batchelor-McAuley, W. Schuhmann and R. G. Compton, *Nano Res.*, 2014, **7**, 71-78.

231.   R. Zhou, Y. Zheng, M. Jaroniec and S.-Z. Qiao, *ACS Catal.*, 2016, **6**, 4720-4728.

232.   K. Kinoshita and P. Stonehart, *Mod. Aspects Electrochem.*, Springer, 1977, pp. 183-266.

233.   K. Kakaei and M. Dorraji, *Electrochim. Acta*, 2014, **143**, 207-215.

234.   X. Wang, W. Wang, Z. Qi, C. Zhao, H. Ji and Z. Zhang, *Int. J. Hydrogen Energy*, 2012, **37**, 2579-2587.

235.   R. N. Singh and C. S. Sharma, *Eng. Technol. Appl. Sci. Res.*, 2012, **2**, 295-301.

236.   T. Nagel, N. Bogolowski and H. Baltruschat, *J. Appl. Electrochem.*, 2006, **36**, 1297-1306.

237.   M. Shao, J. H. Odell, S.-I. Choi and Y. Xia, *Electrochem. Commun.*, 2013, **31**, 46-48.

238.   Z. Jusys, J. Kaiser and R. J. Behm, *Phys. Chem. Chem. Phys.*, 2001, **3**, 4650-4660.

239.   A. Iiyama, S. Iguchi, A. Daimaru and K. Shinohara, 2007. In Fuel cell commercialization conference of Japan.

240.   A. Ohma, K. Shinohara, A. Iiyama, T. Yoshida and A. Daimaru, *ECS Trans.*, 2011, **41**, 775.

241.   Y. Hashimasa and T. Numata, *Int. J. Hydrogen Energy*, 2015, **40**, 11543-11549.

242.   C. Takei, K. Kakinuma, K. Kawashima, K. Tashiro, M. Watanabe and M. Uchida, *J. Power Sources*, 2016, **324**, 729-737.

243.   K. Kakinuma, M. Hayashi, T. Hashimoto, A. Iiyama and M. Uchida, *ACS Appl. Energy Mater.*, 2020, **3**, 6922-6928.

244.   K. Mayrhofer, D. Strmcnik, B. Blizanac, V. Stamenkovic, M. Arenz and N. Markovic, *Electrochim. Acta*, 2008, **53**, 3181-3188.

245.   Y. Garsany, I. L. Singer and K. E. Swider-Lyons, *J. Electroanal. Chem.*, 2011, **662**, 396-406.

246.   I. Takahashi and S. S. Kocha, *J. Power Sources*, 2010, **195**, 6312-6322.

247.   C. Xu, Y. Liu, H. Zhang and H. Geng, *Chem. Asian J.*, 2013, **8**, 2721-2728.

248.   G. W. Sievers, A. W. Jensen, J. Quinson, A. Zana, F. Bizzotto, M. Oezaslan, A. Dworzak, J. J. Kirkensgaard, T. E. Smitshuysen and S. Kadkhodazadeh, *Nat. Mater.*, 2020, 1-6.

249. C. Wan, X. Duan and Y. Huang, *Adv. Energy Mater.*, 2020, **10**, 1903815.

250. D. E. Beltrán and S. Litster, *ACS Energy Lett.*, 2019, **4**, 1158-1161.

251. T. Shinagawa, A. T. Garcia-Esparza and K. Takanabe, *Sci. Rep.*, 2015, **5**, 13801.

252. J. C. Calderón Gómez, R. Moliner and M. J. Lázaro, *Catalysts*, 2016, **6**, 130.

253. L. Jiang, A. Hsu, D. Chu and R. Chen, *J. Electrochem. Soc.*, 2009, **156**, B643.

254. M. Shao, Q. Chang, J.-P. Dodelet and R. Chenitz, *Chem. Rev.*, 2016, **116**, 3594-3657.

255. H. A. Gasteiger, S. S. Kocha, B. Sompalli and F. T. Wagner, *Appl. Catal. B: Environ.*, 2005, **56**, 9-35.

256. C. Chen, *Proceedings of the 10th international conference on Intelligent user interfaces*, 2005, 98-105.

257. C. Chen, F. Ibekwe-SanJuan and J. Hou, *J. Am. Soc. Inf. Sci. Technol.*, 2010, **61**, 1386-1409.